Published in final edited form as:

Cell Rep. 2024 March 26; 43(3): 113852. doi:10.1016/j.celrep.2024.113852.

Species-specific NLRP3 regulation and its role in CNS autoinflammatory diseases

Beverly H. Koller[1,2,6,*], **MyTrang Nguyen**[1,2], **John N. Snouwaert**[1,2], **Christopher A. Gabel**[5], **Jenny P.-Y. Ting**[1,2,3,4,*]

[1]Department of Genetics, University of North Carolina at Chapel Hill, Chapel Hill, NC 27599, USA

[2]Lineberger Comprehensive Cancer Center, University of North Carolina at Chapel Hill, Chapel Hill, NC 27599, USA

[3]Department of Microbiology and Immunology, School of Medicine, University of North Carolina at Chapel Hill, Chapel Hill, NC 27599, USA

[4]Center for Translational Immunology, University of North Carolina at Chapel Hill, Chapel Hill, NC 27599, USA

[5]NodThera, 454 North 34th Street, Seattle, WA 98103, USA

[6]Lead contact

SUMMARY

The NLRP3 inflammasome is essential for caspase-1 activation and the release of interleukin (IL)-1β, IL-18, and gasdermin-D in myeloid cells. However, research on species-specific NLRP3's physiological impact is limited. We engineer mice with the human NLRP3 gene, driven by either the human or mouse promoter, via syntenic replacement at the mouse Nlrp3 locus. Both promoters facilitate hNLRP3 expression in myeloid cells, but the mouse promoter responds more robustly to LPS. Investigating the disease impact of differential NLRP3 regulation, we introduce the D305N gain-of-function mutation into both humanized lines. Chronic inflammation is evident with both promoters; however, CNS outcomes vary significantly. Despite poor response to LPS, the human promoter results in D305N-associated aseptic meningitis, mirroring human pathology. The mouse promoter, although leading to increased CNS expression post-LPS, does not induce meningitis in D305N mutants. Therefore, human-like NLRP3 expression may be crucial for accurate modeling of its role in disease pathogenesis.

*Correspondence: bkoller@email.unc.edu (B.H.K.), jenny_ting@med.unc.edu (J.P.-Y.T.).

AUTHOR CONTRIBUTIONS

Conceptualization, B.H.K., M.N., J.N.S., C.A.G., and J.P.-Y.T. Methodology, B.H.K., M.N., J.N.S., and C.A.G. Formal analysis, M.N., J.N.S., and C.A.G. Investigation, B.H.K., M.N., and J.N.S. Writing – original draft, B.H.K., M.N., and J.N.S. Writing – review & editing, B.H.K., J.N.S., C.A.G., and J.P.-Y.T. Visualization, B.H.K., M.N., and J.N.S. Supervision, B.H.K. and J.P.-Y.T. Funding acquisition, B.H.K. and J.P.-Y.T.

DECLARATION OF INTERESTS

The authors declare no competing interests.

SUPPLEMENTAL INFORMATION

Supplemental information can be found online at https://doi.org/10.1016/j.celrep.2024.113852.

Graphical Abstract

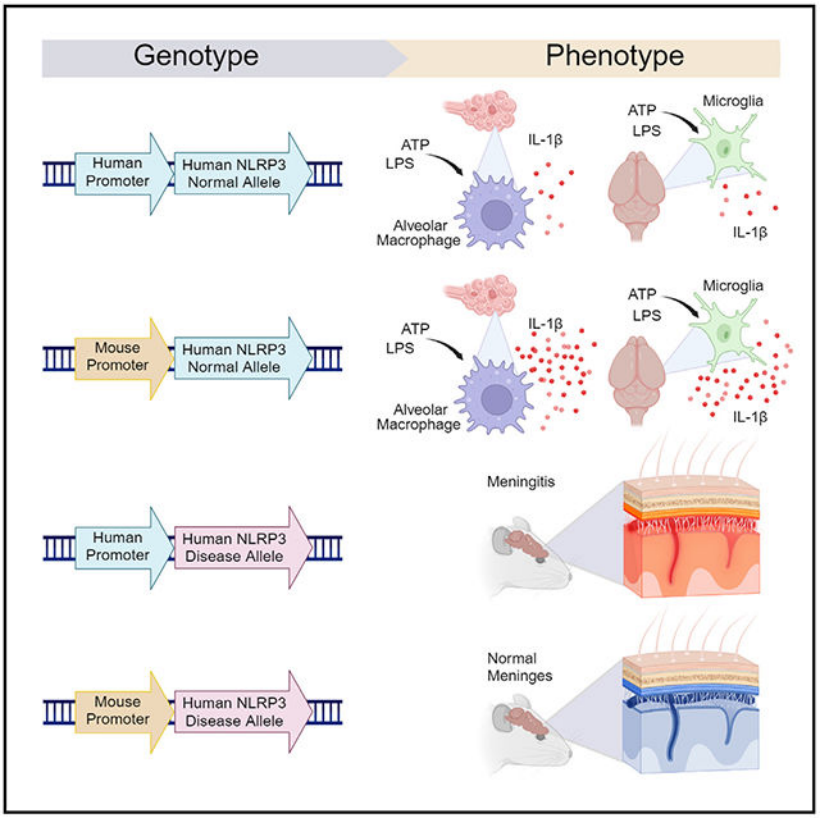

In brief

Koller et al. reveal significant differences in NLRP3 gene expression and LPS responsiveness between humans and mice. Using mice with a gain-of-function mutant NLRP3 driven by mouse or human promoters, they highlight the critical role of NLRP3 expression regulation in immunopathogenesis, particularly in the CNS.

INTRODUCTION

Inflammasomes are pivotal in orchestrating the innate immune response, serving dual functions in cytokine secretion and inflammatory cell survival. Beyond mediating inflammation triggered by endogenous danger signals, they are integral to pathogen-driven immunity.[1-4] These complexes organize around an NLR (nucleotide-binding domain and leucine-rich repeat containing protein) scaffold, promoting the activation of caspase-1, which in turn facilitates the maturation and secretion of the proinflammatory cytokines interleukin-1β (IL-1β) and IL-18.[5-7] Caspase-1 also mediates the cleavage of gasdermin D, essential for pyroptosis, a lytic form of cell death accompanied by the release of the active forms of IL-1β and IL-18.[8]

The activation of the canonical NLRP3 inflammasome involves a two-step process: a priming signal that prepares the cell and an activation signal that triggers its assembly.

This dual-signal model was developed through extensive research using human monocytes, mouse-derived macrophages, and reconstituted nonimmune cell systems.[9,10] Priming often begins with exposure to lipopolysaccharides (LPS) or proinflammatory cytokines, leading to the transcriptional upregulation of NLRP3 via nuclear factor κB (NF-κB).[9] Additional mechanisms such as deubiquitination and phosphorylation also modulate this priming phase.[11,12] Subsequently, various stimuli, including ATP, pore-forming toxins, or cellular metabolites can serve as the second signal, culminating in the full activation of the inflammasome.[13-15] Dysregulations in NLRP3 assembly, as seen in individuals with gain-of-function mutations in NLRP3, underscore the necessity for precise control, as evidenced by the inflammatory conditions associated with such mutations.[15-17]

Two additional mechanisms—noncanonical and alternative inflammasome activation—operate alongside the canonical pathway. In the noncanonical pathway, direct activation of caspase-4/5 or the interaction with caspase-4 by cytoplasmic LPS leads to NLRP3 inflammasome assembly.[18-20] The alternative pathway is characterized by a modest release of mature IL-1β by human monocytes in response to LPS, even without a second signal.[21] Each pathway, still contingent on NLRP3, is susceptible to inhibition by CP456733 (MCC950), demonstrating the central role of NLRP3 in inflammasome formation.[19,22,23]

NLRP3 expression, typically low in resting myeloid cells, is upregulated following exposure to inflammatory signals.[24] Early examinations of the regulatory region of the gene identified myeloid-specific transcription factor sites but not NF-κB sites within the human NLRP3 promoter.[25] However, the role of NF-κB in controlling mouse Nlrp3 expression was shown in bone marrow-derived macrophages (BMDMs).[9] As evidenced by studies using both wild-type and various null mouse line-derived BMDMs, a pathway was proposed in which LPS activates Toll-like receptor 4 (TLR4), enhancing Nlrp3 transcription and NLRP3 protein cytoplasmic levels. Furthermore, two NF-κB sites in the mouse Nlrp3 promoter were identified by electrophoretic mobility shift assay and chromatin immunoprecipitation assays.[26]

The goal of our study here is to determine whether species-specific variations in the NLRP3 5′ regulatory region affect expression and transcriptional priming across different primary myeloid cell populations, thus potentially altering the response of the human and mouse inflammasome to inflammatory stimuli. A second objective of these studies is to assess the pathophysiological relevance of transcriptional regulatory differences in NLRP3, particularly those that differentiate expression of the mouse and human NLRP3 gene. We investigate these issues using mouse models engineered with a humanized NLRP3 locus.

RESULTS

Expression of the human NLRP3 gene in mouse alveolar and peritoneal macrophages (PMs)

We previously reported the generation of mouse lines in which the NLPR3 locus was humanized by syntenic replacement with either the common or a disease associated gain-of-function allele, D305N (amino acid [AA] designation based on Uniprot database),[27] referred to as D303N in early clinical studies. In humans, this mutation results in either

Muckle-Wells syndrome or the more severe autoinflammatory disorder chronic infantile neurological cutaneous and articular syndrome (CINCA).[28,29] Humanization of the locus entailed removal of the 35-kb mouse *Nlrp3* locus from the mouse genome, including 5′ and 3′ flanking DNA. Two mouse lines were generated in which the deleted region was repopulated with a single copy of the corresponding 48-kb segment of human DNA, including the presumed promoter regions, exons, introns and 3′ intergenic DNA. In the first of these lines, the mouse locus was repopulated with human DNA carrying the common *NLRP3* locus. This line is designated hNLRP3 to distinguish it from the *mNlrp3* locus in wild type, control 129 mice. In the second line, the gain-of-function allele D305N was introduced into the human DNA fragment before reconstitution of the locus. This line is designated hD305N (Figure 1A). No difference was observed in the ability of peritoneal macrophages (PMs) from the humanized mice to respond to NLRP3 stimuli with the release of IL-1β.[27]

To examine the relative activity of the NLRP3 inflammasome in additional macrophage populations, we first focused on lung alveolar macrophages (AMs). After establishing parameters for the evaluation of LPS/ATP NLRP3-sensitive release *in vivo* into airways (Figure S1), AMs were collected from mNlrp3, hNLRP3, and hD305N mice via bronchoalveolar lavage (BAL) and primed with LPS (Figure 1). Subsequently, they were treated with either vehicle, ATP, or lethal toxin (LeTx), the latter known to stimulate NLRP1b but not NLRP3.[30] To confirm the response's specificity to NLRP3, some cultures received the NLRP3 inhibitor CP456773 (MCC950) before ATP exposure. LPS-primed mNlrp3 AMs showed significant ATP-induced IL-1β release (Figure 1B). hNLRP3 AMs also released IL-1β upon ATP addition; however, levels were approximately 10% of those from mNlrp3 cells. This response remained CP456773 sensitive. hD305N AMs did not release IL-1β after LPS exposure, consistent with diminished human NLRP3 inflammasome activity. Overall, the IL-1β output in response to LPS/ATP was reduced in hNLRP3 AMs compared to mNlrp3. Cells from mNlrp3, hNLRP3, and hD305N mice showed no difference in response to LeTx, all lines expressing the LeTx-sensitive 129 NLRP1b allele. This suggests that the differences in IL-1β release post-LPS/ATP treatment between hNLRP3 and mNlrp3 lines are due to inherent differences in *NLRP3* expression. To further verify the cell-type-specific difference in the response of AMs and PMs to LPS/ATP, studies were repeated using macrophages from both cells collected from the same animals. (Figure 1C).

To assess *in vivo* NLRP3 inflammasome activity in the lungs, hNLRP3 and hD305N mice were exposed to LPS and ATP by oropharyngeal deposition (OPD) (Figures 1D and 1E). LPS alone failed to increase IL-1β in the BAL fluid (BALF) of mNlrp3 or hNLRP3 mice. Surprisingly, and contrary to our findings on the exposure of the peritoneal cavity to LPS,[27] LPS failed to induce IL-1β release in hD305N lungs. ATP led to high IL-1β levels in the BALF from mNlpr3 lungs. Levels of IL-1β in LPS/ATP-exposed hNLRP3 and hN305N mice were markedly reduced in comparison. Tumor necrosis factor α (TNF-α), chemokine ligand 1, and IL-6 release remained similar across mNlrp3, hNLRP3, and hN305N mice. Thus, the reduced human NLRP3 response of AMs to LPS/ATP translated into a reduced *in vivo* response to these stimuli.

Restoration of the mouse promoter at the humanized NLRP3 locus

We next explored whether the observed activity differences between human and mouse inflammasomes were due to the distinct regulatory expression of *NLRP3/Nlrp3* genes across macrophage populations, which is possibly linked to differences in the human and mouse promoters. To investigate, we generated additional mouse lines in which we restored the DNA segment corresponding to the mouse promoter to the humanized *NLRP3* locus (Figures 2A and 2B). Originally, the human sequence extended approximately 12 kb upstream from the translation start site. In these lines, it is replaced by an 8.3-kb mouse segment that the first humanization event removed. This new embryonic stem cell (ESC)-derived mouse line, called mouse promoter/human NLRP3 (MP-NLRP3), has a mouse-to-human DNA transition just before the start codon (Figure 2A), differentiating it from the fully humanized line (hNLRP3). Two MP-NLRP3 variants were produced: one with the common NLRP3 allele and another with the D305N mutation, called MP-D305N. The relationship of the four lines to one another is depicted by the ideograms in Figure 2B.

Expression of NLRP3 in the MP-NLRP3 mouse

We assessed *NLRP3/Nlrp3* expression in macrophages and tissues from the mNlrp3, hNLRP3, and MP-NLRP3 mice using digital droplet PCR (ddPCR) (Figure 2C). This technique minimizes differences secondary to varying PCR amplification efficiencies.[31] Expression of *NLRP3/Nlrp3* in RNA from lungs and spleen showed minor differences across the lines. Similarly, expression in unstimulated PMs and BMDMs differed little across the three mouse lines. However, AMs from mNlrp3 mice expressed nearly eight times more NLRP3 than the hNLRP3 mice. The difference in expression was also observed in cells from MP-NLRP3 mice, in which the 5′ regulatory region is identical to the mNlpr3 mice. This suggests that in naive AM, other human gene segments such as intronic DNA may determine the level of expression in naive cells. Complicity between promoter and intronic sequences in determining species differences in expression has been noted for other genes, particularly *ACE2*.[32]

NLR3/Nlrp3 levels were similar in RNA prepared from whole brain of the mNlrp3, hNLRP3, and MP-NLRP3 mice (Figure 3D). To determine whether *NLRP3/Nlrp3* expression in the brains of all three lines is largely contributed by immune cells, including microglia, immune cell-enriched populations were prepared from homogenates of mNlrp3, hNLRP3, and MP-NLRP3 brains. Microglia enrichment in these preparations was assessed using the microglial marker *Tmem119* (Figure S2).[33] Expression of *NLRP3/Nlrp3* was increased in these RNA samples from all three lines. This indicates that NLRP3 expression observed in whole brain is highest in immune populations; this basic expression pattern is conserved across species.

Impact of restoration of the mouse *Nlrp3* promoter on NLRP3 activity

We investigated the impact of restoration of the mouse promoter on IL-1β released during LPS/ATP-induced peritonitis. IL-1β levels in the peritoneal lavage fluid collected from the mNlrp3, MP-NLRP3, and hNLRP3 mice were similar (Figure 3A), aligning with previous studies showing comparable activity of the mouse and human NLRP3 inflammasomes in this acute inflammation model.[27] IL-6 levels post-LPS were consistent among the three

groups (Figure 3B). NLRP3 activity in circulating myeloid cells in mNlrp3, hNLRP3, and MP-NLRP3 mice was assessed. Blood collected from the three mouse lines was sequentially stimulated *ex vivo* blood with LPS and ATP.[34] The difference in the promoter regulating *NLRP3* expression had a minimal impact on IL-1β release by blood leukocytes (Figure 3C).

Response of the MP-NLRP3 lung and AMs to LPS/ATP

Restoration of the human promoter increased IL-1β levels in the BALF collected from mice after LPS/ATP exposure (Figure 3D). However, IL-1β levels in the MP-NLRP3 mice remained below the levels measured in mNlpr3 animals. IL-6 levels postairway challenge were similar across all of the mouse lines, albeit being slightly lower in the hNLRP3 and MP-NLRP3 lines (Figure 3E). Consistent with the improved IL1β *in vivo*, AMs collected from the MP-NLRP3 line released higher levels of IL-1β after LPS/ATP stimulation compared to hNLRP3 AMs. In fact, the release was similar to that measured in the supernatant from mNlrp3 AMs (Figure 3F). IL-6 production by AMs collected from all three lines was similar, indicating little difference in sensitivity to LPS (Figure 3G).

Transcriptional priming of NLRP3 in AMs

To examine more closely the attenuated response of AMs from hNLRP3 mice to LPS/ATP, *NLRP3/Nlrp3* expression was determined in AMs collected from mNlrp3, MP-NLRP3, and hNLRP3 pre- and post-LPS exposure (Figure 3H). *Nlrp3* expression was increased after exposure of mNlpr3 AMs to LPS. In contrast, *NLRP3* expression in AMs from NLRP3 changed little post-LPS exposure. MP-NLRP3 AMs, similar to the mNlrp3 AMs, responded to LPS exposure, with a robust increase in *NLRP3* expression. Thus, although restoring the mouse promoter to the humanized locus did not restore basal *NLRP3* expression in AMs (Figure 2C), it did restore LPS-driven transcriptional priming. Induction of the expression of IL-1β, caspase-1, and IL-6 by LPS exposure was similar across all three mouse strains (Figure 3I).

To determine whether differential regulation of human and mouse *NLRP3/Nlrp3* genes was reflected in protein levels, western blot analysis on AM lysates from mNlrp3 mice and two lines in which expression was regulated by the human promoter, hNLRP3 and hD305N, was carried out (Figure 3J). Resting mNlrp3 macrophages showed detectable NLRP3 protein, which increased post-LPS treatment. In contrast, the NLRP3 protein levels in AMs from both hNLRP3 and hD305N lines were below the sensitivity of this assay.

Response of the MP-NLRP3 and hNLRP3 microglial-enriched CNS populations to LPS/ATP

IL-1β release in response to LPS/ATP was assessed in microglia-enriched populations isolated from the brains of mNlrp3, hNLRP3, and MP-NLRP3 animals (Figure 3K). Exposure of these cells to LPS alone resulted in little IL-1β release. The addition of ATP to LPS “primed” cells isolated from mNlrp3 and MP-NLRP3 mice resulted in a dramatic increase in IL-1β release, and the sensitivity of this release to CP456773 verified its dependence on NLRP3 activity. In contrast, the LPS-primed, microglia-enriched population collected from the hNLRP3 mice responded poorly to ATP, showing only a slight increase in IL-1β levels in the collected supernatant. Similar levels of IL-6 release by the three

microglia-enriched populations indicate that this difference does not reflect a variance in cell health or sensitivity to LPS (Figure 3L).

To determine whether this difference in response to LPS/ATP could reflect, at least in part, a difference in the induction of transcription of the *NLRP3/Nlrp3* promoter, mNlrp3, MP-NLRP3, and hNLRP3 mice were treated with a high dose of LPS intravenously, and *NLRP3/Nlrp3* expression in the whole brain was evaluated by qPCR (Figure 3M). An increase in *Nlrp3* expression was observed in mNlrp3 mice. In contrast, no significant change in *NLRP3* expression was detected in brain from LPS-exposed hNLRP3 mice. However, a significant increase in *NLRP3* expression was measured in the MP-NLRP3 mice. Thus, the restoration of the mouse 5′ regulatory region increased the sensitivity of *NLRP3* expression in brain to LPS-mediated transcriptional priming. LPS-mediated induction of *Il6* in the hNLRP3 mice indicates a specific deficit in the induction of NLRP3 expression by LPS in the fully humanized mice (Figure 3L).

Species differences in expression and function of NLRP3 in BMDMs

Research into transcriptional priming and NLRP3 inflammasome assembly and response derives heavily from mouse BMDM studies. High and comparable levels of *NLRP3/Nlpr3* were observed in mNlrp3, hNLRP3, and MP-NLRP3 BMDMs (Figure 2C). Thus, we anticipated a comparable LPS/ATP response across mouse lines. mNlrp3, hNLRP3, and MP-NLRP3 BMDMs were exposed to LPS for 2–18 h, followed by ATP stimulation of the NLRP3 inflammasome and measurement of IL-1β and IL-18 release. IL-18 release was low in all cultures (Figure S4). As expected, a robust and NLRP3-dependent increase in IL-1β release by mNlrp3 BMDMs was observed, peaking at 8 h (Figure 4A). Surprisingly, hNLRP3 BMDMs exhibited negligible IL-1β release at all LPS exposure durations. However, the response to LPS/ATP was completely restored in the MP-NLRP3. IL-6 production remained consistent across all BMDMs, indicating similar LPS responses and cell integrity (Figure 4B).

To determine whether the differential IL-1β release mirrored a species-specific variance in NLRP3 transcriptional priming, we assessed mouse *Nlrp3* and human *NLRP3* expression over time (Figure 4C). *Nlrp3* mRNA levels peaked at 2 h post-LPS and gradually decreased over 24 h but stayed elevated 5-fold compared to naive cells. *NLRP3* expression levels in hNLRP3 BMDM showed no increase over 24 h LPS exposure. In fact, prolonged LPS exposure resulted in a small decrease in in *NLRP3* mRNA levels. *Il6* induction was uniform across BMDMs from all lines. Western blot analysis, performed 2 h post-LPS, revealed low NLRP3 protein in hNLRP3 BMDMs, mirroring their low mRNA levels (Figure 4D). Conversely, MP-NLRP3 BMDMs displayed a substantial NLRP3 increase on LPS exposure, similar to that of the mNlrp3 BMDMs.

Impact of NLRP3 regulation by the mouse promoter on disease pathogenesis

Species differences in the regulation of genes that contribute to innate immunity are not uncommon.[35,36] However, although differences have been noted in basal expression, tissue distribution, and, in some cases, induced expression of genes, it has been far more challenging to assess whether and how these differences affect the pathogenesis of complex

inflammatory diseases. The generation of two mouse lines carrying the gain-of-function NLRP3 allele D305N, differing only in the regulation of this gene, provides a unique opportunity to examine this question. Furthermore, the robust LPS-mediated transcriptional priming, characteristic of mouse but not human NLRP3, allowed this aspect of NLRP3 regulation to be assessed *in vivo*. Our expectation was that because of the higher expression levels of *NLRP3* in some MP-D305N macrophage populations and the LPS sensitivity of the mouse Nlrp3 promoter, this line would show an increase in disease severity relative to the hD305N animals, perhaps reflecting normal environmental exposure to endotoxin. The development of disease was compared in the five mouse lines depicted in the ideogram; the D305N mutant lines corresponding to hNLRP3 and MP-NLRP3 are shown as hatched bars in all of the panels (Figure 5A).

We first examined *in vivo* the acute response of the MP-D305N and hD305N mice to LPS-mediated peritonitis (Figure 5B). MP-D305N and hD305N mice received LPS intraperitoneally, and core body temperatures were monitored over 4 h. A similar sensitivity to LPS was observed in the MP-D305N mice, as reported for hD305N mice.[27] Intraperitoneal LPS exposure resulted in a dramatic drop in core body temperature, which in some cases required the removal of mice from the experiment. IL-1β levels in peritoneal lavage fluid collected at various time points from a parallel group of LPS-exposed animals were similar between the D305N mouse lines (Figure 5C). Thus, the sensitivity of the hD305N and MP-D305N mice to LPS-induced peritonitis paralleled the response of MP-NLRP3 and hNLRP3 mice to LPS/ATP-induced peritonitis (Figure 3A). This likely reflects similar activity of the mouse and human promoter in PMs.

To evaluate chronic inflammation, cohorts of MP-D305N, hD305N, and control lines were bred and cohoused to limit the cage effect.[37] Inflammation was assessed at 7 to 8 months (Figures 5 and S5). The MP-D305N and hD305N were similar in size and growth. We previously reported a small increase in the spleen weight of the hD305N mice compared to mNlrp3 mice.[27] A much greater increase in spleen weight was measured in the MP-D305N (Figure 5D).

The development of visible arthropathy with age is a characteristic of the hD305N mouse line.[27] Mice developed swollen autopods, visible to an experienced observer by 8 weeks, that became more apparent with age. Tissue analysis showed a local increase in cytokines and lipid mediators (Figures 5E and 5F). Surprisingly, the restoration of the LPS-sensitive mouse promoter to the D305N humanized locus did not further exacerbate this aspect of the chronic inflammatory disease of D305N mouse lines. Although increased levels of IL-1β, IL-6, and IL-18 were observed in lysates prepared from MP-D305N autopods compared to their control MP-NLRP3 line, the increase was similar (IL-1β) or in some cases actually slightly lower (IL-6) than cytokine levels in the hD305N mice. Prostaglandin E2 levels were elevated in tissue homogenates from the two mutant lines, but the increase was greater and achieved significance only in the hD305N mice (Figure 5F). Levels of IL-1Ra were elevated in both D305N lines, but again, the increase was greater and achieved significance only for the hD305N line (Figure 5G). Consistent with the presence of an ongoing inflammatory response in the hD305N mice, levels of the major acute-phase protein (APP) serum amyloid P (SAP), encoded by the *Apcs* gene, were elevated (Figure 5H) in these animals. For this

marker, a highly significant increase in plasma SAP levels was observed in the MP-D305N mice compared to the hD305N mice.

To further examine the difference between the MP-D305N and hD305N mice in the induction of expression of APPs, levels of APP transcripts were assessed by qPCR of RNA prepared from the liver. Similar to the increase in SAP, significantly higher levels of *Saa1* (serum amyloid A1) were observed in the MP-D305N mice compared to the hD305N animals (Figure 5I). This was verified using probes that recognized both *Saa1* and *Saa2*. Interestingly, the exuberant increase in APPs in the MP-D305N mice relative to that observed in hD305N mice appeared to be unique to serum amyloid. Although altered expression of other APPs was observed, including an increase in *Lbp* (LPS-binding protein) and *Hp* (haptoglobin), the magnitude of the changes was similar in the hD305N and MP-D305N mice (Figure 5J).

Regulation of NLRP3 by the human promoter drives severe meningitis in mice with the M-W/CIANIA D305N mutation

CNS involvement is observed in some patients who carry Muckle-Wells NLRP3 alleles and the majority of patients with neonatal-onset multisystem nflammatory disease/CINCA syndrome-associated NLRP3 mutations. In view of the robust response of microglia-enriched populations to LPS and the release of high levels of IL-1β by LPS/ATP-treated mNlrp3 and MP-NLRP3 microglia (Figure 3K), we expected that this aspect of the cryopyrin-associated periodic syndromes (CAPs)-associated phenotypes would be enhanced in the MP-D305N mice. To determine whether this was in fact the case, RNA was prepared from whole brain collected from hD305N, MP-D305N, and hNLRP3 animals, and the expression levels of inflammation-associated mRNAs were determined by qPCR. Elevated expression of inflammation-associated genes was observed in RNA prepared from hD305N mice compared to levels in RNA from the hNLRP3 mice. Specifically, the expression of major histocompatibility complex class genes (*H2-Aa and H2-Ab1*), *Nlrc5* (a regulator of class I expression), and the microglial M2-associated gene *Chil3* was significantly elevated in hD305N mice (Figure 5K). The expression of *Ilrn* (IL-1ra) and *Tnf* was also elevated in the brain of hD305N mice. Elevated levels of *Nlrp12*, which is highly expressed in neutrophils,[38] is consistent with increased recruitment of granulocytes in hD305N mice. Compared to the hD305N mice, the mRNA expression of these genes in the MP-D305N mice was significantly lower, showing minimal change from levels observed in control animals. *Gfap* transcripts were also increased in the D305N mice relative to hNLRP3 mice. This gene is expressed in astrocytes in the CNS and is used as a biomarker for gliosis and brain injury. Again, this increase was not observed in the MP-D305N animals. Thus, despite the sensitivity of the MP-NLRP3 promoter to LPS and the robust IL-1β output by microglia in response to LPS/ATP activation, the expression of inflammation markers and *Gfap* was greatly attenuated in the MP-D305N brains relative to that observed in the hD305N animals.

To visualize the difference in CNS involvement between the MP-D305N and hD305N mice, parasagittal sections were prepared from hNLRP3, hD305N, and MP-D305N mice (Figure 6). Representative images from one of the six mice evaluated are shown. Exudates of myeloid cells, including both mononuclear cells and granulocytes, were observed in

the subarachnoid space (SAS) of the hD305N mice (Figures 6C-6F and 6I). Inflammation extended into the sulci and fissures of the brain, following the pia mater (Figure 6I). In contrast, few inflammatory cells were observed in the brain of MP-D305N mice (Figures 6B, 6E, and 6H). In many regions of the hD305N brain, the Virchow-Robin space/perivascular space, which may contribute to the lymphatic system of the brain,[39,40] was populated with myeloid cells (Figures S2A-S2D). In some hD305N animals, neutrophils breached the pia mater and entered into the parenchyma (Figures S2E and S2F).

To further compare the inflammation in the hD305N and MP-D305N mice and to determine whether the increase in cellularity of the SAS and Virchow-Robin space solely reflected an increase in myeloid cells, immune cell populations were isolated from brain homogenates prepared from hD305N, MP-D305N, and hNLRP3 mice and analyzed by flow cytometry (Figure 7). As expected, a major increase in $CD45^+$, $CD11b^+$ cells was observed in the hD305N sample compared to control and MP-D305N samples. However, surprisingly, a large increase in $CD45^+$, $CD11b^-$ cells was also observed in the hD305N mice, suggestive of a recruitment of lymphoid populations secondary to chronic stimulation of the NLRP3 inflammasome.

DISCUSSION

The NLRP3 inflammasome is the most extensively studied mammalian inflammasome. NLRP3 expression is stringently regulated to control innate immune responses in the absence of danger signals. In mouse myeloid cells and certain human cell lines and populations, a rapid increase in *NLRP3* expression and activity upon encountering danger signals is evident. Nevertheless, human NLRP3 expression and regulation have been extrapolated from mouse studies, leading to assumptions of similarity. Contrary to this, our research using mouse models with *NLRP3* controlled by either the mouse or the human 5′ regulatory region, reveals significant differences in mouse and human *Nlrp3/NLRP3* gene expression patterns. These variations in regulation of expression likely stem from adaptive evolutionary modifications in *cis*-regulatory elements due to distinct environmental challenges encountered by the two species.[41] We show that these disparities substantially affect disease pathogenesis.

Our research on NLRP3 activity in mice with *NLRP3* gene expression controlled by either human or mouse promoters centered on its induction by LPS. LPS, used to “prime” the NLRP3 inflammasome, elevates the expression of *NLRP3* and other inflammasome components. LPS binding to TLR4 increases the activity of NF-κB activity, an inducible transcription factor that binds to the κB enhancer in DNA.[42,43] Although the mouse and human 5′ regulatory regions are similar, the κB motif in the mouse is not well conserved in the human sequence. The poor conservation of these motifs is consistent with our finding that the increase in *NLRP3* expression in response to LPS was attenuated in hNLRP3 AMs, BMDMs, and microglia-enriched myeloid cells compared to similar populations derived from mice in which *NLRP3* was regulated by the mouse promoter. However, LPS/ATP responses varied among myeloid cell populations.

Upon exposure of peritoneal and blood leukocytes from hNLRP3 mice to LPS/ATP, a significant increase in IL1-β release was noted, with a 10-fold rise in *NLRP3* mRNA in PMs. This suggests that LPS-mediated transcriptional priming of NLRP3 can occur in some myeloid populations. In PMs, additional transcription factors may enhance binding to the suboptimal κB site, a process that possibly is absent in other myeloid types. Such cofactor protein cooperation at promoter and enhancer elements is known.[44-46] We cannot discount that NLRP3 priming in certain cells may partly rely on autocrine pathways.[47] The absence of LPS priming in some myeloid cells may stem from the structure of the human regulatory region, where human chromatin configuration may restrict transcription factor access to motifs in a cell-type-specific manner.[48] In addition, an unidentified negative regulatory motif that limits NF-κB motif binding could exist in the human 5′ regulatory region, with the corresponding transcription factor being cell type specific. Differences in the 5′ regulatory region between species extend beyond conservation of the κB site. The human promoter contains an Ets/interferon regulatory factor (IRF) composite motif for PU.1 and IRF8/IRF4 at −309/−300 which is absent in mice, whereas the Ets motif at +5/+8 is conserved. Empirical data highlight the role of these motifs in NLRP3 expression regulation in THP-1 and U937 cells and human peripheral blood-derived macrophages.[49]

Mice expressing a gain-of-function *NLRP3* D305N mutant allele, controlled by human or mouse promoters, offer insights into the impact of *NLRP3* transcriptional regulation on disease pathogenesis. Crucially, differences observed in the D305N lines cannot be attributed to species-specific posttranscriptional modifications, substrate interactions, regulatory protein interactions, or protein turnover and ubiquitination.[50] In addition, miRNA regulation, such as regulation of NLRP3 by interaction of miR-223 with the 3′ UTR, is expected to be identical in both lines.[51]

The unexpected finding that disease progression was not exacerbated in MP-D305N mice implies that despite the likely presence of LPS in the environment,[52] LPS-mediated transcriptional priming of *NLRP3/Nlrp3* may not be crucial in the development of chronic inflammation. However, PMs and blood monocytes from both human CAPs patients and D305N mice release IL-1β in response to very low LPS levels. This sensitivity may be due to LPS-induced expression of other inflammasome components and IL-1β.[53]

Sterile meningitis in severe cases of CAPs is characterized by elevated cytokines (IL-1β, IL-6, TNF) and an increase in monocytes and granulocytes in the cerebrospinal fluid (CSF).[54,55] Similar observations were made in hD305N mice, where brain mRNA analysis revealed heightened inflammation markers and histological study showed granulocytes and other leukocytes in the SAS. In contrast, inflammation was less pronounced in the same tissue of the MP-D305N mouse line. Fluorescence-activated cell sorting (FACS) analysis of immune populations in the brain further supported the variation in the manifestation of this aspect of autoinflammatory disease between the two D305N mouse lines. This difference may be due to the unique requirements of the human promoter for optimal NLRP3 expression in myeloid cells. This expression pattern may be crucial for monitoring and responding to damage-associated molecular patterns/pathogen-associated molecular patterns at the blood-CSF barrier and the arachnoid barrier. The variations in NLRP3

regulation between humans and mice could reflect the adaptation of each species to its unique physiology, immune response, or pathogen susceptibility.[56]

The increasing recognition of brain myeloid populations, including the barrier-associated macrophages (BAMs) crucial for immunosurveillance at various blood-brain barriers, has been propelled by single-cell sequence analysis of immune populations and enhanced understanding of the embryonic origin of certain myeloid subgroups.[57-61] Recent studies have also uncovered substantial complexity within these populations, including cell composition changes following postviral infection repopulation.[62-64] Macrophages in the Virchow-Robins/perivascular space are thought to aid in the presentation of antigens collected from the interstitial parenchymal space to T cells.[40] In this regard it is interesting that we also noted an increase in nonmyeloid ($CD11^{-}/CD45^{+}$) cells in the hD305N line. Given the pivotal role of BAMs and other myeloid cells in immune surveillance, regulation of NLRP3 expression likely aligns with their distinct functions and CNS locations.[65]

In conclusion, although the structural conservation of the NLRP3 protein in humans and mice suggests a similar IL-1β processing function, our study highlights the need to consider species-specific transcriptional regulation differences of *NLRP3/Nlrp3* when assessing its role in autoinflammatory and autoimmune diseases. The significant role of the mouse NLRP3 inflammasome in a disease model may not be directly comparable to its role in the corresponding human disease. Conversely, the uniquely regulated human inflammasome could play a crucial role in diseases in which inhibition of the mouse NLRP3 inflammasome does not mitigate disease progression. Using mice with *NLRP3* regulation more reflective of human conditions could enhance the predictive value of mouse models in developing therapies targeting diseases influenced by this inflammasome.

Limitations of the study

We cannot dismiss the possibility that some phenotypic differences observed between the hD305N mouse and the MP-D305N mouse within the CNS could be due to transcriptional alterations unique to this particular mouse line; variations may not accurately reflect gene expression patterns in humans. Such a model would require that interactions between mouse transcription factors and the human promoter are increased, leading to enhanced expression in certain cell types. However, it is generally expected that the interactions between mouse transcription factors/regulatory elements with the human enhancer/promoter region would be similar, or in some cases perhaps less efficient, potentially resulting in reduced, not enhanced, expression when expression is driven by mouse regulatory elements. Furthermore, the occurrence of meningitis in the mouse model closely parallels that seen in individuals with NLRP3-related autoinflammatory disorders. This resemblance implies that the severe meningitis in the hD305N mice is related to differences intrinsic to the human 5′ regulatory region. Although this supports a model in which human transcriptional regulation, intrinsic to the human promoter, is critical for these phenotypes, we cannot entirely dismiss this alternative hypothesis.

The impact of varying sensitivities to LPS transcriptional priming between humans and mice on the pathogenesis of other NLRP3-dependent inflammatory diseases remains unexplored in our studies. Due to the ubiquitous nature of LPS, its exposure level in mice likely

varies significantly based on their environment. Our findings indicate that this variation may lead to enhanced transcriptional priming in mice, amplifying the role of NLRP3 in certain inflammatory models. Although our research highlights the species-specific differences in LPS sensitivity during acute inflammation caused by LPS/ATP, it does not examine the broader implications of these differences on LPS promoter sensitivity outside of this autoinflammatory context. Consequently, a limitation of our studies is the extent to which we can generalize these findings, especially when using wild-type mice to understand the role of NLRP3 in complex inflammatory responses in disease models such as those for multiple sclerosis and Alzheimer's disease.

STAR★METHODS

RESOURCE AVAILABILITY

Lead contact—Further information and requests for resources and reagents should be directed to and will be fulfilled by the lead contact, Beverly Koller (bkoller@email.unc.edu).

Materials availability—Cell lines and mouse lines generated in this study will be freely available upon request.

Data and code availability

- All data reported in this paper will be shared by the lead contact upon request.
- This paper does not report original code.
- Any additional information required to reanalyze the data reported in this work paper is available from the lead contact upon request.

EXPERIMENTAL MODEL AND STUDY PARTICIPANT DETAILS

Animal breeding and housing—Animal experimentation at the University of North Carolina at Chapel Hill complies with U.S. Department of Agriculture guidelines, the National Institutes of Health Guide for the Care and Use of Laboratory Animals, and is approved by the Institutional Animal Care and Use Committee (IACUC). Mice are housed in a pathogen-free environment with individually ventilated caging (Tecniplast Green Line GM500), irradiated bedding (Bed o' Cob 14″), and fed LabDiet -PICOLAB Select,5V5R irradiated PMI Nutrition International *ad libitum*. The cage environment is enriched with both Nestlets (Ancare). In addition, each cage has a "mouse house" (Tecniplast) that allows only red wavelength light to pass through. As mice lack red light receptors, this provides an additional feeling of security and decreases stress. Drinking water is purified by reverse osmosis and provided via an automatic system. All mice are bred and reared at UNC-Chapel Hill under consistent conditions, with various genotypes cohabited when possible to ensure uniform microenvironment exposure.

Generation of mice carrying a humanized NLRP3 locus—Generation of mouse ESCs and mouse lines lacking the entire 35-kb mouse *Nlrp3* locus, extending from base pair 59,534,790 to base pair 59,569,921 on chromosome 11, has been reported previously. To generate mice in which expression of NLRP3 was driven by the mouse upstream promoter,

the *ΔNlrp3* locus was corrected by insertion of a segment of DNA encoding human NLRP3 as described previously,[27] except in this case the segment of DNA consisted of mouse genomic DNA upstream of the start codon (chr11:59,534,766-59,543,112) followed by human coding and downstream sequences (chr1:247,418,795-247,455,018). The segment of mouse genomic DNA was derived from the bMQ221G10 clone from the bMQ 129 mouse library. The segment of human DNA was derived from the RP11-243D8 clone from the RPCI-11 human BAC library. The two segments of DNA were incorporated into the previously described Replacer vector using standard recombineering techniques. The genotype of MP-NLRP3 mice was confirmed by PCR across the upstream mouse-human junction.

Isolation and culture of peritoneal, alveolar and bone marrow-derived macrophages (BMDM)—Peritoneal macrophages were collected by lavage of the peritoneal cavity with 4 mL of Hank's buffer without Ca2+ and Mg2+. Cells were allowed to adhere to petri dishes in macrophage culture medium (RPMI 1640, 10% FBS, 10 mM HEPES, 2 mM L-glutamine, 1X penicillin/streptomycin, and 0.1 mM μME) at 37°C in a 5% $C0_2$ incubator. After 2 h of incubation, petri dishes were washed 3X with culture medium to removed non-adherent cells. Macrophages were then detached from petri dishes using cold PBS/10 mM EDTA. Cells were counted, plated in a 96-well flat bottom culture plates at a density of $1X10^5$ cells/well in culture medium, and incubated overnight before stimulation.

Alveolar macrophages were obtained by bronchoalveolar lavage (BAL). Briefly, lungs were perfused with PBS via pulmonary artery until they turned light pink. Lungs were then lavaged 5 times with 1 mL of lavage buffer (PBS with 0.5% FBS and 0.5 mM EDTA). Bronchoalveolar lavage fluid (BALF) was collected from between 3 and 10 mice of identical genotype to generate a unique sample. The number of mice used to generate a pool was dependent on the number of cells required based on experiment design. In experiments with multiple pools, cells from additional groups of animals were collected to generate additional unique pools of the same genotype. After pooling the BALF was then centrifuged at 300 x g for 5 min at 4°C, resuspended in macrophage culture medium, and cultured overnight at a density of $1 X 10^5$ cells/well in 96-well plates before treatment.

Bone marrow-derived macrophages (BMDMs) were differentiated as previously reported.[30] Briefly, bone marrow hematopoietic stem cells from the femurs and tibias of mice were flushed with 10 mL of Hank's buffered saline supplemented with 25 mM HEPES and 50 μg/mL of gentamicin. Cells were collected by centrifugation at 300 x g for 5 min at room temperature and cultured in TC plates in BMDM complete medium (DMEM with 10% FCS, 15% L929-conditioned medium which contains macrophage colony stimulating factor, 100 mM sodium pyruvate, 1 mM NEAA, 2 mM L-glutamine, 1X penicillin/streptomycin, 0.1 mM βME, and 50 μg/mL gentamycin) at 37°C in a 5% $C0_2$ incubator. After 24 h of incubation, non-adherent cells were transferred to non-tissue culture Petri dishes and cultured continually in BMDM complete medium for 7 days. After 7 days, BMDMs were detached from Petri dishes using cold PBS/10 mM EDTA and cultured in a 96-well plate at $1 x 10^5$ cells/well in BMDM complete medium without L929-conditoned medium overnight before initiating treatment.

Isolation of mouse microglia—Microglia were isolated as described previously.[66] Briefly, each perfused brain was diced into small pieces and transferred to a 15-mL tube containing 3 mL of dissociation medium [DMEM/F12, 1 mg/mL Papain, 1.2 U/mL Dispase II and 20 U/mL DNase I for 20 min at 37°C with gentle inversion every 5 min. At the end of the incubation period, 5 mL of neutralization media (DMEM/F12, 10% FBS and 4.5 μg/mL glucose) was added to the tube to neutralize the enzymes, followed by 5 min of centrifugation at 250 x g. Pelleted tissues were resuspended in 6 mL of DMEM/F12 media and dissociated by pipetting up and down using a Pasteur pipette. Cell suspension was then passed through a 40 μm cell strainer. The filtered cell suspension was centrifuged at 250 x g for 4 min. Cell pellet was resuspended in 4 mL of 37% isotonic Percoll, and 4 mL of 70% isotonic Percoll was gently underlaid. Then 4 mL of 30% isotonic Percoll was overlaid gently on top of the 37% layer, followed by 2 mL of PBS. The gradient was centrifuged at 300 x g for 40 min at 18°C with no brake. Cell enriched for immune cells, primarily microglia, were collected at the 37–70% interface, washed once with PBS, and isolated for RNA and functional assays.

METHOD DETAILS

Treatments—See Table S1 for list of Figures/panels in each figure and corresponding dose and exposure time. General information for the methods is provided here. To induce cytokine release from macrophages, microglia and BMDM cells were primed for 4–5 h (or time indicated in Table S1)with 1 μg/mL of LPS in culture medium, and some cells were pre-treated with 1 μM of CP456773/MCC950 for 30 min before ATP stimulation. Cells were then pulsed with 5 mM ATP for 30 min. For cytokine induction by anthrax lethal toxin (LeTx), LPS-primed cells were treated with LeTx at a final concentration of 250 ng/mL (LF and PA) for 3 h. Cell supernatants were collected and frozen at −80°C until assayed.

LPS/ATP-induced release of IL-1β in peritoneum—mNlrp3, hNLRP3 and MP-NLRP3 mice received an intraperitoneal (i.p.) injection of 1 μg per mouse of LPS (Escherichia coli serotype 055:B5). After 2 h of LPS injection, mice received a second i.p. injection of either 500 μL of 30 mM ATP or PBS. At 30-min post-ATP challenge, mice were euthanized, and the peritoneal cavity was lavaged with 3 mL of PBS. Peritoneal fluids were centrifuged, and supernatants were collected for cytokine analysis. For hD305N and MP-D305N mice the LPS dose was reduced to 0.25 mg/kg (i.p.)

LPS/ATP-induced release of IL-1β in lung airways—Mice were anesthetized under isoflurane and exposed to 0.3 mg/kg of LPS (Escherichia coli serotype 055:B5) in 50 μL of sterile phosphate buffered saline (PBS) by oropharyngeal deposition (OPD). Some animals were treated by intraperitoneal injection with CP456773/MCC950 (50 mg/kg) 1 h prior to LPS exposure. After 2 h of LPS challenge, mice were given 50 μL of 100 mM ATP by OPD. After 2 h of ATP administration, mice were euthanized and BALF collected via lung lavage. BALF free of cells was frozen at −80°C until assayed.

LPS/ATP-whole blood assay—Blood was collected via the left ventricle using a 26-gauge needle and immediately transferred to an eppendorf tube containing 10 units of heparin. Heparinized blood was diluted with RPMI 1640 containing 20 mM HEPES, pH 7.3

at a dilution ratio of 1:0.5. LPS was added to diluted blood at a concentration of 1 μg/mL. LPS-treated blood was then transferred to a 96-well plate (190 μL/well) and incubated for 3 h at 37°C. After the 3 h LPS priming, 10 μL of 100 mM ATP (5 mM final concentration) was added to the wells and incubated for another 30 min at 37°C. At the end of incubation period, the plate was centrifuged, and plasma supernatants were recovered for cytokine analysis.

LPS treatment of mice prior to tissue collection—For evaluation of the *in vivo* response and induction of gene expression in the CNS, LPS (Escherichia coli serotype 055:B5) was delivered by i.v. (tail vein) injections. Mice received10 mg/kg of LPS and tissue was collected for RNA analysis 2 h after LPS exposure.

Cytokine and LDH measurements—Cytokine levels in cell supernatants and cell-free BAL fluids were determined by commercial enzyme-linked immunosorbent assay (ELISA) kits according to the manufacturer's instructions. Lactate dehydrogenase (LDH) levels, an indicator of cytotoxicity, in BALF were measured using the Cytotoxicity Detection Kit.

Western blotting—Macrophages were either untreated or treated with LPS (1 μg/mL) for time indicated in Table S1, at 37°C. Cells were washed twice with cold PBS and lysed in 200 μL of lysis buffer (10 mM Tris-HCl, 150 mM NaCl and 1% Triton X-100), containing 1 mM EDTA, 1 mM sodium Na3VO4, 1 mM DTT, 1 mM PMSF, and complete protease inhibitor tablet. After lysing on ice with gentle shaking for 30 min, the cell lysates were cleared by centrifugation at 15,000 g for 10 min at 4°C. The proteins were quantified by the Bradford method. Cell lysates containing an equal amount of protein were resolved by electrophoresis on 8% polyacrylamide gels. The proteins were transferred electrophoretically to Immobile-P membrane. After blocking in 10 mM Tris-HCl (pH 8.0) containing 150 mM sodium chloride, 0.1% Tween 20, and 5% (w/v) nonfat dry milk, the membrane was treated with appropriate primary antibodies, followed by incubation with horseradish peroxidase-conjugated secondary antibodies. The antigen–antibody complexes were detected using the ECL chemiluminescence reagent kit. The antibodies used in this study were anti NLRP3 (Cryo-2) (1:1000) and β-actin (1:1000). Relative density of NLPR3/Cryo-2 was quantified using NIH ImageJ software. The density of each non-saturated band was measured, normalized to β-actin loading control, and expressed as a ratio of NLRP3/Cryo-2 over control.

Droplet digital PCR (ddPCR)—Total RNA was isolated from various tissues and macrophages using RNA STAT-60 as previously described.[32] High-Capacity cDNA Reverse Transcription kit (Applied Biosystems, Foster City, CA) was used to generate cDNA from RNA. ddPCR reactions were performed with QX200 Droplet Digital PCR System (Bio-Rad, Hercules, CA) according to the manufacturer's instructions. Each reaction mixture (20 μL) contained 10 μL ddPCR Supermix for Probes (No dUTP) (Bio-Rad), 5 μL of template cDNA, 1 μL of Primers/Probes (900 nM per primer and 250 nM probe) and 4 μL of ddH20. The reaction mixtures were loaded into a disposable droplet generator cartridge (Bio-Rad), and droplets were formed using Bio-Rad QX-100 emulsification device. The contents were transferred to a 96-well plate and sealed with foil using Eppendorf 96-well heat sealer. PCR

amplification of the droplets was performed using a C1000 Touch Thermal Cycler (Bio-Rad) with the following parameters: 95°C for 10 min, followed by 40 cycles of 94°C for 30 s and 60°C for 1 min, and a final 98°C for 10 min. After PCR amplification, the plate was scanned using a QX200 Droplet Reader (Bio-Rad). QX Manager Software (Bio-Rad) was used to analyze the data by calculating the absolute copy number of the target DNA (units of copies/μL) using Poisson distribution analysis. All TaqMan gene expression probes were purchased.

Quantitative real-time PCR—qPCR was carried out as previously detailed.[67] For BMDM expression analysis, cells were treated with 1 μg/mL of LPS and collected at various time points. Total RNA was then isolated from treated BMDMs using RNA STAT-60 according to the instruction manual. Reverse transcription of total RNA to cDNA for quantitative real-time PCR was performed by using a High-Capacity cDNA Reverse Transcription kit according to the manufacturer's instructions. Primers and probes were purchased. All reactions were performed with TaqMan PCR Universal Master Mix using the Applied Biosystems QuanStudio 6 Flex Real-Time PCR System. Reactions were carried out in duplicate in a 20 μL final volume reaction. PCR conditions for all reactions were as follows: 2 min at 50°C and 10 min at 95°C, followed by 40 cycles at 95°C for 15 s and 60°C for 1 min. Expression levels of genes of interest were normalized to 18S. Data were analyzed using the comparative C_T method as described by Applied Biosystems.

Histology—Mice were euthanized, the skull removed, and one hemisphere snap frozen for mRNA isolation and the second fixed by submersion in 10% phosphate buffered formalin for 7 days. The hemisphere was embedded in paraffin and parasagittal sections prepared at 3 μM thickness. Sections were stained with hematoxylin and eosin.

Flow cytometry—Isolated microglial enriched populations (2×10^5 cells) were isolated and stained with purified CD16/32 antibody in FACS buffer (PBS with 2% FBS) for 15 min at 4°C to block the Fc receptors prior to antibody staining to minimize non-specific staining. Following blocking incubation, cells were stained with fluorescent-conjugated antibodies against surface markers for 40 min at 4°C in the dark. Cells were then washed twice with FACS buffer to remove unbound antibodies and re-suspended in FACS buffer for flow cytometric analysis. Data were acquired (5×10^4 cells) on an Attune NxT flow cytometer (Thermo Fisher Scientific). Compensation matrices for correcting spectral overlap were automatically calculated using single-stain controls on the Attune NxT cytometric software. The data were analyzed using FlowJo data analysis software (FlowJo, LLC, Ashland, CA), version 10.6.1.

QUANTIFICATION AND STATISTICAL ANALYSIS

The data are presented as mean ± SEM. The biological sample, "N," is shown in brackets below each bar with the exception of Figure 5. Because of the complexity of this figure, the number of samples (N) in each panel is shown in tabular form in Figure S5. Data were analyzed by one-way or two-way ANOVA depending on the number of variables in the experiment (treatment and genotype), followed by Tukey's multiple comparisons test. Gubbs' test was applied for removal of outliers. Because of the complexity of Figures

3 and 5, and to allow possible comparison between the multiple genotypes, statistics for experiment/panel is provided in the Supplemental Excel file. The statistical method used for data analysis is included in each figure and the accompanying figure legend. Means with a P-value of less than 0.05 were considered statistically significant. Statistics were performed using GraphPad Prism.

Supplementary Material

Refer to Web version on PubMed Central for supplementary material.

ACKNOWLEDGMENTS

We thank Carolyn Suitt at the Center for Gastrointestinal Biology and Disease Histology Core (P30 DK34987). We thank Alexa V. Rayle for genotyping. We thank Anne Latour for ESC tissue culture work. This work is supported by NIH grant R01AI158314 to J.P.-Y.T. and B.H.K. and R21AI166471 to B.H.K. B.H.K. is supported in part by UM1HG012003. We thank Michael Love, Jon Rosen, and Folami Ideraabdulla for support in the genetic analysis of regulatory regions across species. The University of North Carolina (UNC) Flow Cytometry Core Facility (RRID: SCR_019170) is supported in part by the P30 CA016086 Cancer Center Core Support Grant to the UNC Lineberger Comprehensive Cancer Center.

REFERENCES

1. Jorgensen I, Rayamajhi M, and Miao EA (2017). Programmed cell death as a defence against infection. Nat. Rev. Immunol 17, 151–164. 10.1038/nri.2016.147. [PubMed: 28138137]
2. Trindade BC, and Chen GY (2020). NOD1 and NOD2 in inflammatory and infectious diseases. Immunol. Rev 297, 139–161. 10.1111/imr.12902. [PubMed: 32677123]
3. Diamond MS, and Kanneganti TD (2022). Innate immunity: the first line of defense against SARS-CoV-2. Nat. Immunol 23, 165–176. 10.1038/s41590-021-01091-0. [PubMed: 35105981]
4. Juge-Aubry CE, Somm E, Chicheportiche R, Burger D, Pernin A, Cuénod-Pittet B, Quinodoz P, Giusti V, Dayer JM, and Meier CA (2004). Regulatory effects of interleukin (IL)-1, interferon-beta, and IL-4 on the production of IL-1 receptor antagonist by human adipose tissue. J. Clin. Endocrinol. Metab 89, 2652–2658. 10.1210/jc.2003-031219. [PubMed: 15181037]
5. Ting JPY, Lovering RC, Alnemri ES, Bertin J, Boss JM, Davis BK, Flavell RA, Girardin SE, Godzik A, Harton JA, et al. (2008). The NLR gene family: a standard nomenclature. Immunity 28, 285–287. 10.1016/j.immuni.2008.02.005. [PubMed: 18341998]
6. Broz P, and Dixit VM (2016). Inflammasomes: mechanism of assembly, regulation and signalling. Nat. Rev. Immunol 16, 407–420. 10.1038/nri.2016.58. [PubMed: 27291964]
7. Amer AO (2011). The inflammasome. Front. Microbiol 2, 4. 10.3389/fmicb.2011.00004. [PubMed: 21713058]
8. Fu J, and Wu H (2023). Structural Mechanisms of NLRP3 Inflammasome Assembly and Activation. Annu. Rev. Immunol 41, 301–316. 10.1146/annurev-immunol-081022-021207. [PubMed: 36750315]
9. Bauernfeind FG, Horvath G, Stutz A, Alnemri ES, MacDonald K, Speert D, Fernandes-Alnemri T, Wu J, Monks BG, Fitzgerald KA, et al. (2009). Cutting edge: NF-kappaB activating pattern recognition and cytokine receptors license NLRP3 inflammasome activation by regulating NLRP3 expression. J. Immunol 183, 787–791. 10.4049/jimmunol.0901363. [PubMed: 19570822]
10. Zito G, Buscetta M, Cimino M, Dino P, Bucchieri F, and Cipollina C (2020). Cellular Models and Assays to Study NLRP3 Inflammasome Biology. Int. J. Mol. Sci 21, 4294. 10.3390/ijms21124294. [PubMed: 32560261]
11. Elliott EI, Miller AN, Banoth B, Iyer SS, Stotland A, Weiss JP, Gottlieb RA, Sutterwala FS, and Cassel SL (2018). Cutting Edge: Mitochondrial Assembly of the NLRP3 Inflammasome Complex Is Initiated at Priming. J. Immunol 200, 3047–3052. 10.4049/jimmunol.1701723. [PubMed: 29602772]

12. Seok JK, Kang HC, Cho YY, Lee HS, and Lee JY (2020). Regulation of the NLRP3 Inflammasome by Post-Translational Modifications and Small Molecules. Front. Immunol 11, 618231. 10.3389/fimmu.2020.618231. [PubMed: 33603747]
13. Cassel SL, and Sutterwala FS (2010). Sterile inflammatory responses mediated by the NLRP3 inflammasome. Eur. J. Immunol 40, 607–611. 10.1002/eji.200940207. [PubMed: 20201012]
14. Muñoz-Planillo R, Kuffa P, Martínez-Colón G, Smith BL, Rajendiran TM, and Núñez G (2013). K(+) efflux is the common trigger of NLRP3 inflammasome activation by bacterial toxins and particulate matter. Immunity 38, 1142–1153. 10.1016/j.immuni.2013.05.016. [PubMed: 23809161]
15. Kastner DL, Aksentijevich I, and Goldbach-Mansky R (2010). Autoinflammatory disease reloaded: a clinical perspective. Cell 140, 784–790. 10.1016/j.cell.2010.03.002. [PubMed: 20303869]
16. Lin B, and Goldbach-Mansky R (2022). Pathogenic insights from genetic causes of autoinflammatory inflammasomopathies and interferonopathies. J. Allergy Clin. Immunol 149, 819–832. 10.1016/j.jaci.2021.10.027. [PubMed: 34893352]
17. Henderson C, and Goldbach-Mansky R (2010). Monogenic IL-1 mediated autoinflammatory and immunodeficiency syndromes: finding the right balance in response to danger signals. Clin. Immunol 135, 210–222. 10.1016/j.clim.2010.02.013. [PubMed: 20353899]
18. Downs KP, Nguyen H, Dorfleutner A, and Stehlik C (2020). An overview of the non-canonical inflammasome. Mol. Aspects Med 76, 100924. 10.1016/j.mam.2020.100924. [PubMed: 33187725]
19. Baker PJ, Boucher D, Bierschenk D, Tebartz C, Whitney PG, D'Silva DB, Tanzer MC, Monteleone M, Robertson AAB, Cooper MA, et al. (2015). NLRP3 inflammasome activation downstream of cytoplasmic LPS recognition by both caspase-4 and caspase-5. Eur. J. Immunol 45, 2918–2926. 10.1002/eji.201545655. [PubMed: 26173988]
20. Abu Khweek A, and Amer AO (2020). Pyroptotic and non-pyroptotic effector functions of caspase-11. Immunol. Rev 297, 39–52. 10.1111/imr.12910. [PubMed: 32737894]
21. Gaidt MM, Ebert TS, Chauhan D, Schmidt T, Schmid-Burgk JL, Rapino F, Robertson AAB, Cooper MA, Graf T, and Hornung V (2016). Human Monocytes Engage an Alternative Inflammasome Pathway. Immunity 44, 833–846. 10.1016/j.immuni.2016.01.012. [PubMed: 27037191]
22. Perregaux DG, McNiff P, Laliberte R, Hawryluk N, Peurano H, Stam E, Eggler J, Griffiths R, Dombroski MA, and Gabel CA (2001). Identification and characterization of a novel class of interleukin-1 post-translational processing inhibitors. J. Pharmacol. Exp. Ther 299, 187–197. [PubMed: 11561079]
23. Coll RC, Robertson AAB, Chae JJ, Higgins SC, Muñoz-Planillo R, Inserra MC, Vetter I, Dungan LS, Monks BG, Stutz A, et al. (2015). A small-molecule inhibitor of the NLRP3 inflammasome for the treatment of inflammatory diseases. Nat. Med 21, 248–255. 10.1038/nm.3806. [PubMed: 25686105]
24. Guarda G, Zenger M, Yazdi AS, Schroder K, Ferrero I, Menu P, Tardivel A, Mattmann C, and Tschopp J (2011). Differential expression of NLRP3 among hematopoietic cells. J. Immunol 186, 2529–2534. 10.4049/jimmunol.1002720. [PubMed: 21257968]
25. Anderson JP, Mueller JL, Misaghi A, Anderson S, Sivagnanam M, Kolodner RD, and Hoffman HM (2008). Initial description of the human NLRP3 promoter. Genes Immun. 9, 721–726. 10.1038/gene.2008.66. [PubMed: 18719602]
26. Qiao Y, Wang P, Qi J, Zhang L, and Gao C (2012). TLR-induced NF-kappaB activation regulates NLRP3 expression in murine macrophages. FEBS Lett. 586, 1022–1026. 10.1016/j.febslet.2012.02.045. [PubMed: 22569257]
27. Snouwaert JN, Nguyen M, Repenning PW, Dye R, Livingston EW, Kovarova M, Moy SS, Brigman BE, Bateman TA, Ting JPY, and Koller BH (2016). An NLRP3 Mutation Causes Arthropathy and Osteoporosis in Humanized Mice. Cell Rep. 17, 3077–3088. 10.1016/j.celrep.2016.11.052. [PubMed: 27974218]
28. Abdulla MC, Alungal J, Hawkins PN, and Mohammed S (2015). Muckle-Wells syndrome in an Indian family associated with NLRP3 mutation. J. Postgrad. Med 61, 120–122. 10.4103/0022-3859.153107. [PubMed: 25766347]

29. Feldmann J, Prieur AM, Quartier P, Berquin P, Certain S, Cortis E, Teillac-Hamel D, Fischer A, and de Saint Basile G (2002). Chronic infantile neurological cutaneous and articular syndrome is caused by mutations in CIAS1, a gene highly expressed in polymorphonuclear cells and chondrocytes. Am. J. Hum. Genet 71, 198–203. 10.1086/341357. [PubMed: 12032915]
30. Kovarova M, Hesker PR, Jania L, Nguyen M, Snouwaert JN, Xiang Z, Lommatzsch SE, Huang MT, Ting JPY, and Koller BH (2012). NLRP1-dependent pyroptosis leads to acute lung injury and morbidity in mice. J. Immunol 189, 2006–2016. 10.4049/jimmunol.1201065. [PubMed: 22753929]
31. Vossen RHAM, and White SJ (2017). Quantitative DNA Analysis Using Droplet Digital PCR. Methods Mol. Biol 1492, 167–177. 10.1007/978-1-4939-6442-0_11. [PubMed: 27822863]
32. Snouwaert JN, Jania LA, Nguyen T, Martinez DR, Schäfer A, Catanzaro NJ, Gully KL, Baric RS, Heise M, Ferris MT, et al. (2023). Human ACE2 expression, a major tropism determinant for SARS-CoV-2, is regulated by upstream and intragenic elements. PLoS Pathog. 19, e1011168. 10.1371/journal.ppat.1011168. [PubMed: 36812267]
33. Bennett ML, Bennett FC, Liddelow SA, Ajami B, Zamanian JL, Fernhoff NB, Mulinyawe SB, Bohlen CJ, Adil A, Tucker A, et al. (2016). New tools for studying microglia in the mouse and human CNS. Proc. Natl. Acad. Sci. USA 113, E1738–E1746. 10.1073/pnas.1525528113. [PubMed: 26884166]
34. Primiano MJ, Lefker BA, Bowman MR, Bree AG, Hubeau C, Bonin PD, Mangan M, Dower K, Monks BG, Cushing L, et al. (2016). Efficacy and Pharmacology of the NLRP3 Inflammasome Inhibitor CP-456,773 (CRID3) in Murine Models of Dermal and Pulmonary Inflammation. J. Immunol 197, 2421–2433. 10.4049/jimmunol.1600035. [PubMed: 27521339]
35. Hagai T, Chen X, Miragaia RJ, Rostom R, Gomes T, Kunowska N, Henriksson J, Park JE, Proserpio V, Donati G, et al. (2018). Gene expression variability across cells and species shapes innate immunity. Nature 563, 197–202. 10.1038/s41586-018-0657-2. [PubMed: 30356220]
36. Donnard E, Vangala P, Afik S, McCauley S, Nowosielska A, Kucukural A, Tabak B, Zhu X, Diehl W, McDonel P, et al. (2018). Comparative Analysis of Immune Cells Reveals a Conserved Regulatory Lexicon. Cell Syst. 6, 381–394.e7. 10.1016/j.cels.2018.01.002. [PubMed: 29454939]
37. Hildebrand F, Nguyen TLA, Brinkman B, Yunta RG, Cauwe B, Vandenabeele P, Liston A, and Raes J (2013). Inflammation-associated enterotypes, host genotype, cage and inter-individual effects drive gut microbiota variation in common laboratory mice. Genome Biol. 14, R4. 10.1186/gb-2013-14-1-r4. [PubMed: 23347395]
38. Ulland TK, Jain N, Hornick EE, Elliott EI, Clay GM, Sadler JJ, Mills KAM, Janowski AM, Volk APD, Wang K, et al. (2016). Nlrp12 mutation causes C57BL/6J strain-specific defect in neutrophil recruitment. Nat. Commun 7, 13180. 10.1038/ncomms13180. [PubMed: 27779193]
39. Mestre H, Mori Y, and Nedergaard M (2020). The Brain's Glymphatic System: Current Controversies. Trends Neurosci. 43, 458–466. 10.1016/j.tins.2020.04.003. [PubMed: 32423764]
40. Ineichen BV, Okar SV, Proulx ST, Engelhardt B, Lassmann H, and Reich DS (2022). Perivascular spaces and their role in neuroinflammation. Neuron 110, 3566–3581. 10.1016/j.neuron.2022.10.024. [PubMed: 36327898]
41. Emerson JJ, and Li WH (2010). The genetic basis of evolutionary change in gene expression levels. Philos. Trans. R. Soc. Lond. B Biol. Sci 365, 2581–2590. 10.1098/rstb.2010.0005. [PubMed: 20643748]
42. Poltorak A, He X, Smirnova I, Liu MY, Van Huffel C, Du X, Birdwell D, Alejos E, Silva M, Galanos C, et al. (1998). Defective LPS signaling in C3H/HeJ and C57BL/10ScCr mice: mutations in Tlr4 gene. Science 282, 2085–2088. 10.1126/science.282.5396.2085. [PubMed: 9851930]
43. Hoshino K, Takeuchi O, Kawai T, Sanjo H, Ogawa T, Takeda Y, Takeda K, and Akira S (1999). Cutting edge: Toll-like receptor 4 (TLR4)-deficient mice are hyporesponsive tob lipopolysaccharide: evidence for TLR4 as the Lps gene product. J. Immunol 162, 3749–3752. [PubMed: 10201887]
44. Mulero MC, Shahabi S, Ko MS, Schiffer JM, Huang DB, Wang VYF, Amaro RE, Huxford T, and Ghosh G (2018). Protein Cofactors Are Essential for High-Affinity DNA Binding by the Nuclear Factor kappaB RelA Subunit. Biochemistry 57, 2943–2957. 10.1021/acs.biochem.8b00158. [PubMed: 29708732]

45. Grivennikov SI, and Karin M (2010). Dangerous liaisons: STAT3 and NF-kappaB collaboration and crosstalk in cancer. Cytokine Growth Factor Rev. 21, 11–19. 10.1016/j.cytogfr.2009.11.005. [PubMed: 20018552]
46. Zeitlinger J. (2020). Seven myths of how transcription factors read the cis-regulatory code. Curr. Opin. Syst. Biol 23, 22–31. 10.1016/j.coisb.2020.08.002. [PubMed: 33134611]
47. Lee TK, Denny EM, Sanghvi JC, Gaston JE, Maynard ND, Hughey JJ, and Covert MW (2009). A noisy paracrine signal determines the cellular NF-kappaB response to lipopolysaccharide. Sci. Signal 2, ra65. 10.1126/scisignal.2000599. [PubMed: 19843957]
48. Wei M, Wang L, Wu T, Xi J, Han Y, Yang X, Zhang D, Fang Q, and Tang B (2016). NLRP3 Activation Was Regulated by DNA Methylation Modification during Mycobacterium tuberculosis Infection. BioMed Res. Int 2016, 4323281. 10.1155/2016/4323281. [PubMed: 27366746]
49. Yashiro T, Yamamoto M, Araumi S, Hara M, Yogo K, Uchida K, Kasakura K, and Nishiyama C (2021). PU.1 and IRF8 Modulate Activation of NLRP3 Inflammasome via Regulating Its Expression in Human Macrophages. Front. Immunol 12, 649572. 10.3389/fimmu.2021.649572. [PubMed: 33897697]
50. Tang J, Tu S, Lin G, Guo H, Yan C, Liu Q, Huang L, Tang N, Xiao Y, Pope RM, et al. (2020). Sequential ubiquitination of NLRP3 by RNF125 and Cbl-b limits inflammasome activation and endotoxemia. J. Exp. Med 217, e20182091. 10.1084/jem.20182091. [PubMed: 31999304]
51. Haneklaus M, Gerlic M, Kurowska-Stolarska M, Rainey AA, Pich D, McInnes IB, Hammerschmidt W, O'Neill LAJ, and Masters SL (2012). Cutting edge: miR-223 and EBV miR-BART15 regulate the NLRP3 inflammasome and IL-1beta production. J. Immunol 189, 3795–3799. 10.4049/jimmunol.1200312. [PubMed: 22984081]
52. Mohr AE, Crawford M, Jasbi P, Fessler S, and Sweazea KL (2022). Lipopolysaccharide and the gut microbiota: considering structural variation. FEBS Lett. 596, 849–875. 10.1002/1873-3468.14328. [PubMed: 35262962]
53. Kelley N, Jeltema D, Duan Y, and He Y (2019). The NLRP3 Inflammasome: An Overview of Mechanisms of Activation and Regulation. Int. J. Mol. Sci 20, 3328. 10.3390/ijms20133328. [PubMed: 31284572]
54. Rodriguez-Smith J, Lin YC, Tsai WL, Kim H, Montealegre-Sanchez G, Chapelle D, Huang Y, Sibley CH, Gadina M, Wesley R, et al. (2017). Cerebrospinal Fluid Cytokines Correlate With Aseptic Meningitis and Blood-Brain Barrier Function in Neonatal-Onset Multisystem Inflammatory Disease: Central Nervous System Biomarkers in Neonatal-Onset Multisystem Inflammatory Disease Correlate With Central Nervous System Inflammation. Arthritis Rheumatol. 69, 1325–1336. 10.1002/art.40055. [PubMed: 28118536]
55. Han S, Lin YC, Wu T, Salgado AD, Mexhitaj I, Wuest SC, Romm E, Ohayon J, Goldbach-Mansky R, Vanderver A, et al. (2014). Comprehensive immunophenotyping of cerebrospinal fluid cells in patients with neuroimmunological diseases. J. Immunol 192, 2551–2563. 10.4049/jimmunol.1302884. [PubMed: 24510966]
56. Sadekar SS, Bowen M, Cai H, Jamalian S, Rafidi H, Shatz-Binder W, Lafrance-Vanasse J, Chan P, Meilandt WJ, Oldendorp A, et al. (2022). Translational Approaches for Brain Delivery of Biologics via Cerebrospinal Fluid. Clin. Pharmacol. Ther 111, 826–834. 10.1002/cpt.2531. [PubMed: 35064573]
57. Galea I. (2021). The blood-brain barrier in systemic infection and inflammation. Cell. Mol. Immunol 18, 2489–2501. 10.1038/s41423-021-00757-x. [PubMed: 34594000]
58. Ghersi-Egea JF, Strazielle N, Catala M, Silva-Vargas V, Doetsch F, and Engelhardt B (2018). Molecular anatomy and functions of the choroidal blood-cerebrospinal fluid barrier in health and disease. Acta Neuropathol. 135, 337–361. 10.1007/s00401-018-1807-1. [PubMed: 29368213]
59. Jordão MJC, Sankowski R, Brendecke SM, Sagar, Locatelli G, Tai YH, Tay TL, Schramm E, Armbruster S, Hagemeyer N, et al. (2019). Single-cell profiling identifies myeloid cell subsets with distinct fates during neuroinflammation. Science 363, eaat7554. 10.1126/science.aat7554. [PubMed: 30679343]
60. Dani N, Herbst RH, McCabe C, Green GS, Kaiser K, Head JP, Cui J, Shipley FB, Jang A, Dionne D, et al. (2021). A cellular and spatial map of the choroid plexus across brain ventricles and ages. Cell 184, 3056–3074.e21. 10.1016/j.cell.2021.04.003. [PubMed: 33932339]

61. Herz J, Filiano AJ, Wiltbank AT, Yogev N, and Kipnis J (2017). Myeloid Cells in the Central Nervous System. Immunity 46, 943–956. 10.1016/j.immuni.2017.06.007. [PubMed: 28636961]

62. Song E, and Iwasaki A (2019). Monocytes Inadequately Fill In for Meningeal Macrophages. Trends Immunol. 40, 463–465. 10.1016/j.it.2019.04.004. [PubMed: 31072686]

63. Rua R, Lee JY, Silva AB, Swafford IS, Maric D, Johnson KR, and McGavern DB (2019). Infection drives meningeal engraftment by inflammatory monocytes that impairs CNS immunity. Nat. Immunol 20, 407–419. 10.1038/s41590-019-0344-y. [PubMed: 30886419]

64. Derk J, Jones HE, Como C, Pawlikowski B, and Siegenthaler JA (2021). Living on the Edge of the CNS: Meninges Cell Diversity in Health and Disease. Front. Cell. Neurosci 15, 703944. 10.3389/fncel.2021.703944. [PubMed: 34276313]

65. Mildenberger W, Stifter SA, and Greter M (2022). Diversity and function of brain-associated macrophages. Curr. Opin. Immunol 76, 102181. 10.1016/j.coi.2022.102181. [PubMed: 35462276]

66. Lee JK, and Tansey MG (2013). Microglia isolation from adult mouse brain. Methods Mol. Biol 1041, 17–23. 10.1007/978-1-62703-520-0_3. [PubMed: 23813365]

67. Koller BH, Snouwaert JN, Douillet C, Jania LA, El-Masri H, Thomas DJ, and Stýblo M (2020). Arsenic Metabolism in Mice Carrying a BORCS7/AS3MT Locus Humanized by Syntenic Replacement. Environ. Health Perspect 128, 87003. 10.1289/EHP6943. [PubMed: 32779937]

Highlights

- Mouse lines are generated as a platform to compare NLRP3 and Nlrp3 regulation
- In contrast to mouse, the human NLRP3 promoter responds poorly to LPS in most cells
- The impact of differential NLRP3 regulation on inflammation is organ specific
- Severe sterile meningitis develops in mice with human NLRP3-D305N expression patterns

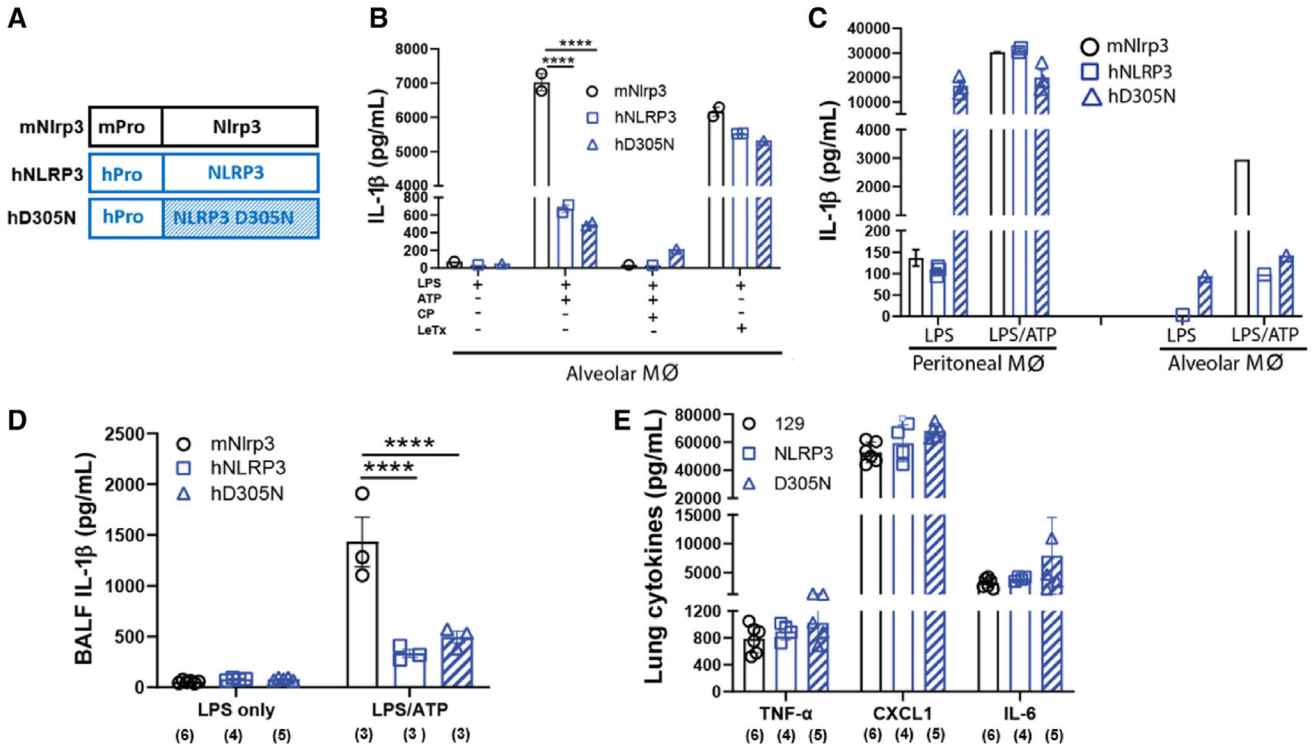

Figure 1. Activity of human and mouse NLRP3 inflammasomes in peritoneal and AMs

(A) Ideogram showing the promoter and coding region, color-coded for humanized and wild-type mouse lines. Hatched bars indicate the D305N mutation.

(B) AM samples pooled from mice, with 2 pools in the study. Cells were primed with LPS and then stimulated with ATP or LeTx. Some cultures were pretreated with CP456773 before ATP. The treatment regimen is detailed beneath the graph.

(C) Comparison of IL-1β release in response to LPS/ATP between peritoneal and AMs from the same mice showed differential responses. AMs were pooled from mice of each genotype. PMs were collected from 3 of 4 mice contributing to the AM sample.

(D and E) *In vivo* response of hNLRP3 and mNlrp3 mice to LPS and ATP assessed. Mice received OPD of LPS, followed by ATP or vehicle OPD. BALF was collected for assessment of IL-1β (D) and other cytokine/chemokine (E) levels by ELISA. For LPS, ATP, LeTx, CP456733 doses, and exposure times see STAR Methods.

Results are mean ± SEM. *p < 0.05; ***p < 0.001; ****p < 0.0001.

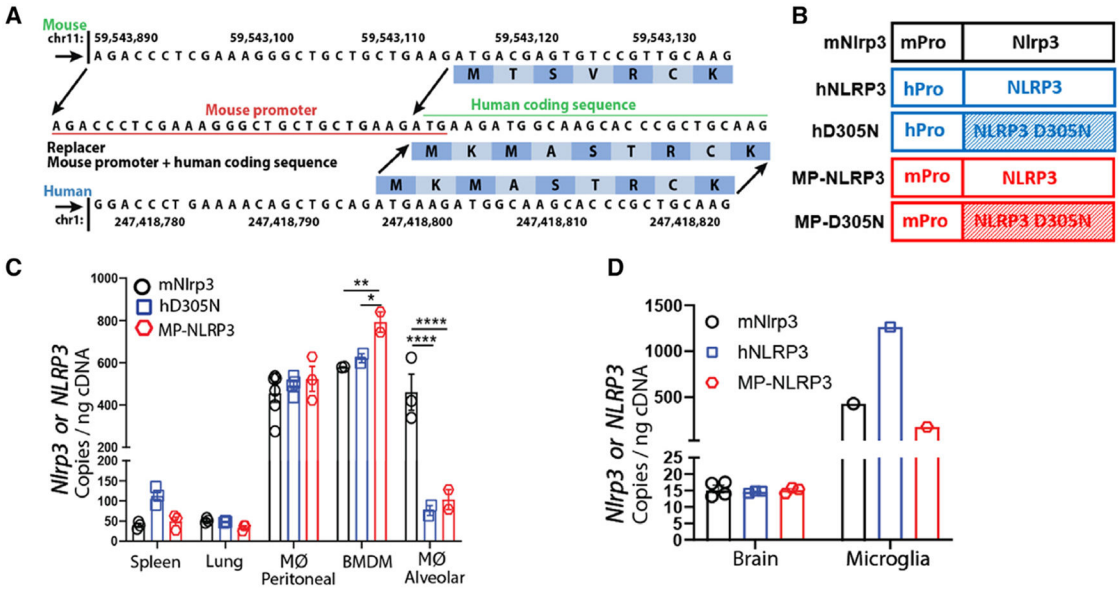

Figure 2. Mouse promoter restoration in humanized locus

(A) Junction between mouse promoter and human sequence is shown. The alignment preserves mouse regulatory sequences and human codons.

(B) Ideogram illustrating the structure for the MP-NLRP3 and MP-D305 loci compared to mNlrp3, hNLRP3, and hD305N mice. The color assignment used throughout the report is shown. Hatched bars indicate the mutant allele.

(C) ddPCR comparison of *Nlrp3* or *NLRP3* expression in specified tissues and myeloid cells.

(D) Similar *NLRP3/Nlrp3* expression levels are observed across mouse lines in whole brain. For all 3 lines, higher expression is observed in RNA prepared from whole-brain resident immune cells, a population enriched for microglial cells (see Figure S2).

Results are mean ± SEM. *p < 0.05; **p < 0.01; ***p < 0.001.

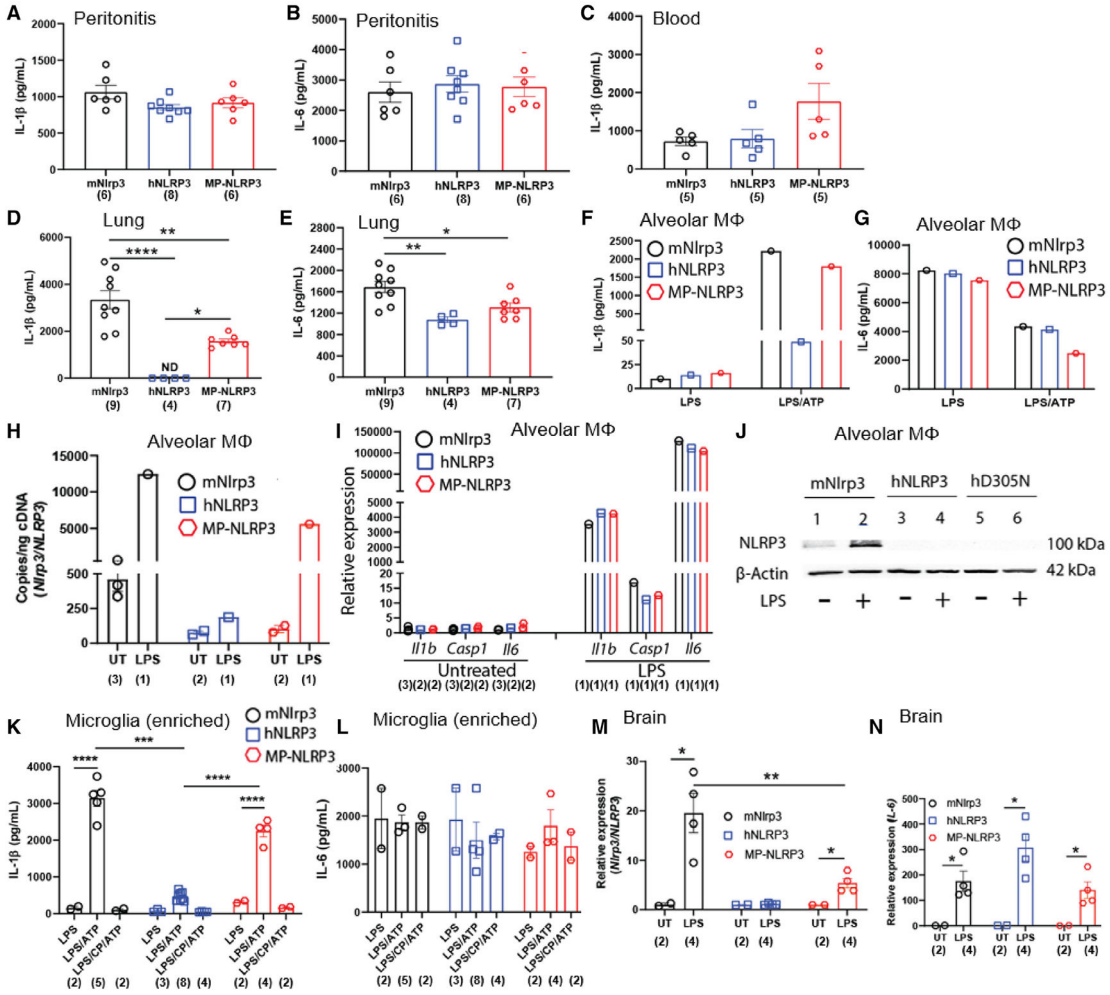

Figure 3. Mouse promoter restoration affects IL-1β release in response to LPS/ATP across tissues

(A and B) IL-1β (A) and IL-6 (B) levels measured in peritoneal fluid from mice with indicated genotypes, post-LPS and ATP exposure (intraperitoneal).

(C) Blood stimulated with LPS and ATP was analyzed for IL-1β release.

(D and E) Following OPD exposure to LPS/ATP, IL-1β (D) and IL-6 (E) levels in the BALF were determined.

(F and G) Pools of AMs were exposed to LPS alone or LPS followed by ATP and IL-1β (F) and IL-6 (G) release measured.

(H and I) Expression of *NLRP3/Nlrp3* (H) and other LPS-sensitive transcripts (I) in naive and LPS-treated AMs by ddPCR.and qPCR.

(J) Western blot analysis of human and mouse NLRP3 proteins in naive and LPS-exposed AMs. β-Actin reprobing of the membrane shows protein levels. For expanded image, see Figure S3.

(K and L) Microglial-enriched immune cell populations isolated from whole brain were stimulated with LPS and LPS/ATP. Indicated cultures were treated with CP456773 (CP). IL-1β (K) and IL-6 (L) levels in supernatant were determined.

(M and N) Gene expression in the brain of naive mice and post-intravenous LPS exposure, quantified by qPCR, with naive levels assigned a value of 1. See STAR Methods and Table S1 for doses/and exposure times.

Results are mean ± SEM. *p < 0.05; **p < 0.01; ***p < 0.001. Group sizes are shown below the bars. For statistical methods and additional intergroup comparisons, see Table S2.

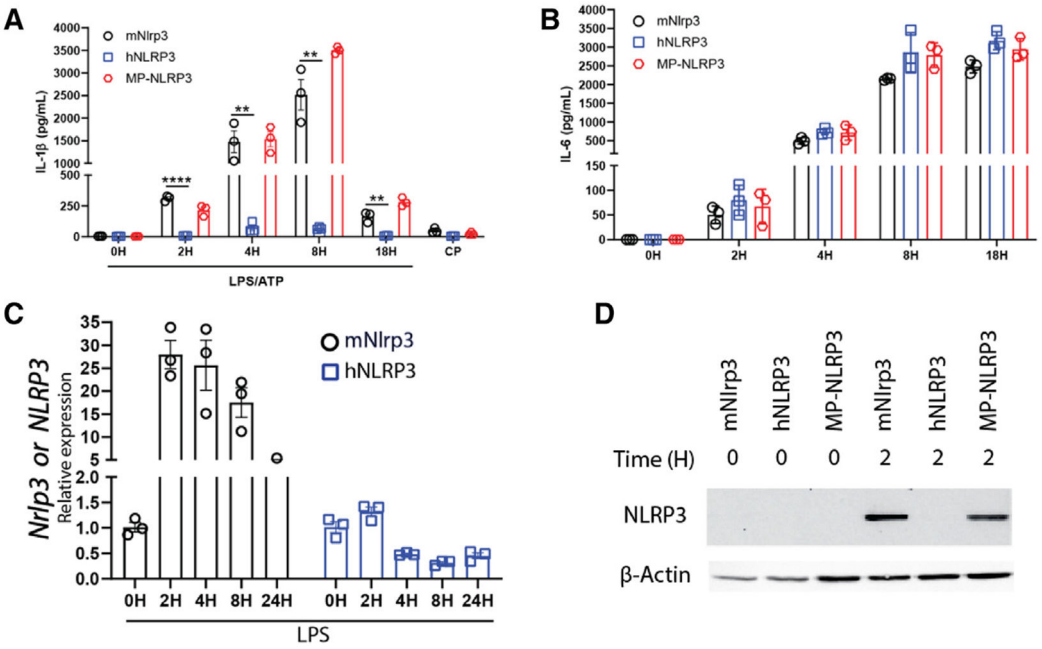

Figure 4. NLRP3-dependent cytokine release in BMDM cultures

(A–C) BMDMs were established from mNlrp3, MP-NLRP3, and hNLRP3 mice (3 cultures from 3 mice/genotype). (A and B) Cells were stimulated with LPS for indicated time and then exposed to ATP. IL-1β and IL-6 (B) levels in culture medium were measured by ELISA. The 4-h time point was duplicated to verify NLRP3-dependent IL-1β release by CP456773 (CP) treatment. (C) Post-LPS treatment, mRNA from BMDMs was converted to cDNA for *NLRP3* or *Nlrp3* qPCR analysis, normalized to 18S RNA, and expressed as fold change from the 0 time point.

(D) BMDM NLRP3 protein levels compared by western blot. Lysates pre- and 2 h post-LPS exposure analyzed with an NLRP3 antibody recognizing both human and mouse proteins. Filter was reprobed with β-actin to verify protein loading. For expanded gel image, see Figure S3. For IL-18 release, see Figure S4.

Results are mean ± SEM. **p < 0.01; ***p < 0.001; ****p < 0.0001.

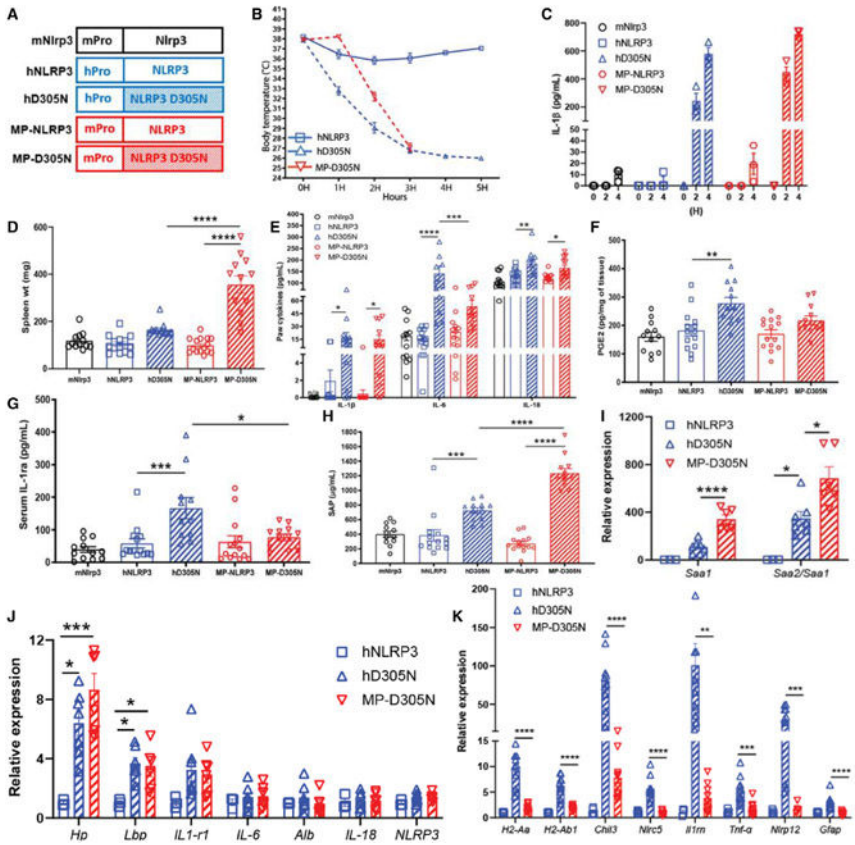

Figure 5. Autoinflammatory disease in D305N and MP-D305N mice

(A) Ideogram/color key illustrating the *Nlrp3/NLRP3* locus structure. Hatched bars indicate D305N mutation in mouse lines.

(B) Mice of indicated genotypes received LPS intraperitoneally, and the core body temperature was monitored over 5 h.

(C) IL-β levels in peritoneal fluid of a similarly treated cohort were measured at 2 and 4 h post-LPS exposure.

(D–F) Spleen weights (D), (E) cytokines, and (F) PGE_2 levels in homogenates of autopods from the 5 mouse lines.

(G) Serum IL-1ra levels in mice of indicated genotypes.

(H) Increase in major APP and SAP, determined by ELISA.

(I) Liver serum amyloid A (*Saa1* and *Saa2*) mRNA/cDNA, determined by a *Saa1*-specific probe or a probe recognizing *Saa1* and *Saa2*.

(J) Expression of additional APPs, *Hps, Lbp*, cytokines, and *Nlrp3/NLRP3* in liver.

(K) hD305N show elevated expression of inflammatory markers and *Gfap*, an astrogliosis marker, compared to both hNLRP3 and MP-D305N mice.

Alb, albumin; *Chil3*, chitinase-like 3; *Gfap*, glial fibrillary acid protein; *Hp*, haptoglobin; *Il1r1*, IL-1 receptor 1; *Il6*, IL-6; *Il1rn*, IL-1 receptor antagonist; *Lbp*, lipopolysaccharide binding protein; *Tnf*, tumor necrosis factor.

Results expressed as mean ± SEM. *p < 0.05; **p < 0.01; ***p < 0.001; ****p < 0.0001. See Figure S5 for age of mice and Table S1 for additional comparison of statistical differences between the 5 mouse lines.

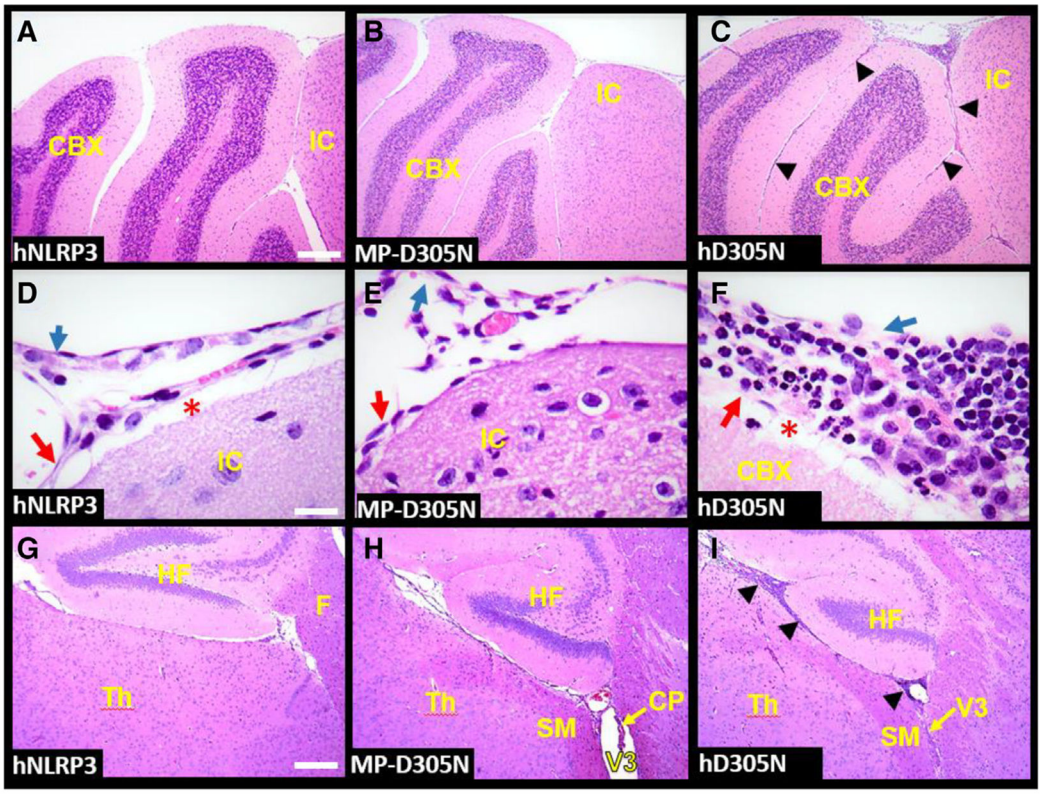

Figure 6. The human promoter drives inflammation in the leptomeninges of mice carrying the D305N mutation

(A and B) Sagittal sections of brains from the indicated mouse lines show a CSF-filled SAS covering the cerebellum and midbrain and extending from the brain surface into the physiological openings, including the transverse fissure located between the midbrain and cerebellum and the primary and secondary fissures that define the cerebellar lobes and lobules (arrow-heads). As expected, few cells can be observed in the SAS in hNLRP3 (A) and MP-D305N (B) mice.

(C–E) Increased magnification of this region of the hNLRP3 (D) and MP-D305N (E) brain shows an SAS defined by the arachnoid mater (blue arrows) and the delicate pia mater (red arrows) that cover the brain surface and follow the brain parenchyma along the fissures and other physiological openings. In contrast, in the hD305N mice, accumulation of inflammatory cells is apparent, both at the surface of the brain and in the SAS that extends into the transverse and cerebellar fissures (C).

(F) At high magnification, both mononuclear cells and granulocytes, identified by their multi-lobular nucleus, are observed in the SAS of the hD305N mice. Inflammation in the hD305N mouse is not limited to the cerebellar/midbrain region.

(G–I) In the hNLRP3 (G) and MP-D305N (H) brains, few inflammatory cells can be seen in the SAS because it extends from the surface of the brain between the cerebrum and midbrain to the tela choroidea of the third ventricle. In contrast, in the hD305N mice, inflammatory cells are found throughout this region (arrowheads), including in the SAS immediately dorsal to the roof of the third ventricle (I). Sections are representative of histological changes observed in 6 mice of each genotype. See Figure S6 for additional images of hD305N mice.

White bars: 200 μm in (A–C) and (G–I), and 50 μm in (D–F). CBX, cerebellum; CP, choroid plexus; F, fornix; HF, hippocampal formation; IC, inferior colliculus; SM, stria medullaris; Th, thalamus; V3, third ventricle. Red asterisk indicates the separation of the pia mater from the brain parenchyma, a common histological artifact.

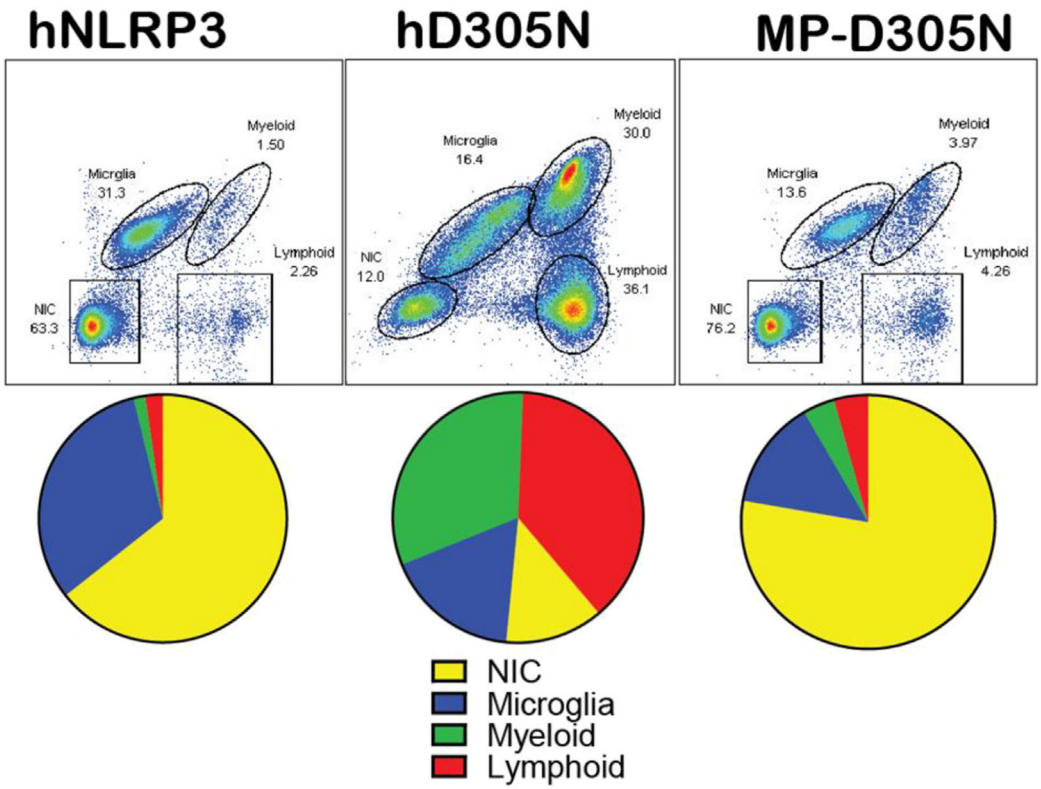

Figure 7. Immune profiling of leukocyte subpopulations in the brains of MP-D305N and hD305N mice

Cell fractions enriched for leukocytes were collected by Percoll gradient from homogenates prepared from the brain and leptomeninges of 4 female 5-month-old mice of the indicated genotype. CD45 was used to identify leukocytes, which were further defined as myeloid, microglia, or lymphoid, based on CD45 and CD11b expression. X axis, CD45; Y axis, CD11b. For the gating strategy, see Figure S7. NIC, non-immune cells. .

KEY RESOURCES TABLE

REAGENT or RESOURCE	SOURCE	IDENTIFIER
Antibodies		
anti-NLRP3/NALP3, mAb (Cryo-2)	AdipoGen Life Sciences	AG-20B-0014-C100
Anti-β-actin	Biolegend	Cat# 643801; RRID: AB_2223201
Anti-mouse-IgG HRP	Cell Signaling Technology	Cat# 7076; RRID: AB_330924
Anti-mouse-CD16/32	Biolegend	Cat# 101302; RRID: AB_312800
Anti-CD11b	Biolegend	Cat# 101237; RRID: AB_2565431
Anti-CD45	Biolegend	Cat* 103107; RRID: AB_312972
Chemicals, peptides, and recombinant proteins		
Hank's Balanced Salt Solution	Gibco (ThermoFisher)	14175–095
DMEM/F-12 Medium	Gibco (ThermoFisher)	11320033
RPMI 1640	Gibco	11875–093
Fetal Bovine Serum	VWR	97068–085
HEPES	Corning	25–060-Cl
L-glutamine	Gibco (ThermoFisher)	25030–81
Penicillin/streptomycin	Gibco (ThermoFisher)	10378016
βME	Sigma-Aldrich	M3148
Dulbecco's Phosphate Buffered Saline (PBS)	Sigma	S8537
Heparin 1000U/ml	Sargent Pharmaceuticals	118703
EDTA	Sigma-Aldrich	D8537
Gentamycin	Gibco (ThermoFisher)	15710064
L929 conditioned medium	ATCC	CCL-1
LPS (Escherichia coli serotype 055:B5)	Sigma-Aldrich	L2637
CP456773	Sigma-Aldrich	PZ0280
ATP	Sigma	A3377
Anthrax lethal toxin	List Biological Laboratories Inc.	#171B/#172B
Isoflurane (Forane)	Baxter	NDC-10019-360-60
NEAA	Gibco (ThermoFisher)	Cat #11140050
Triton X-100	Sigma-Aldrich	X100
Sodium Na3VO4	Sigma	S-6508
Sodium Pyruvate (100 mM)	Gibco	Cat # 11-360-070
DTT	Roche Diagnostics	10-197-777-001
PMSF	Sigma	P-7626
Complete Protease Inhibitor Cocktail	Millipore-Sigma	Cat #11697498001
Immobilon-P	Millipore-Sigma	IPVH00005
Tween 20	Fisher	BP337
Instant NoFat Dry Milk	Market Pantry	Target Corporation
Applied Biosystem TaqMan Universal PCR Master Mix	Applied Biosystems	Cat #43-044-37
Phosphate buffered formalin	Fisher	245685
ddPCR Supermix for Probes (no dUTP)	Biorad	1863023
Papain	Sigma	P 3125

REAGENT or RESOURCE	SOURCE	IDENTIFIER
Dispase II	Sigma	04 942 078 001
Dnase I	Sigma-Aldrich	DN25
Percoll	Sigma-Aldrich	P1644
RNA STAT-60	Tel-Test Inc.	CS-502
Critical commercial assays		
IL-1β ELISA Kit	R&D Systems	DY401
IL-1ra/IL-1F13 ELISA	R&D Systems	MRA00
CXCL1/KC DuoSet-ELISA	R&D Systems	DY453
TNF-α ELISA Kit	Invitrogen	88-7324-88
IL-18 ELISA Kit	Invitrogen	BMS618-3
Il-6 ELISA Kit	R&D Systems	M600B
Cytotoxicity Detection Kit (LDH)	Roche Diagnostics	Cat #11644793001
BioRad Protein Assay Kit	Bio-Rad	5000002
Pierce ECL Western Blotting Detection Kit	Thermo	32209
RNA STAT-60	Tel Test, Inc.	Cat #CS-502
Taqman PCR Universal Master Mix	Thermofisher	Cat #4304437
High-Capacity cDNA Reverse Transcription kit	Applied Biosystems	Cat #4368814
TaqMan™ Gene Expression Assay (FAM), Mouse Hp	Thermofisher	Mm00516884_m1
TaqMan™ Gene Expression Assay (FAM), Mouse Lbp	Thermofisher	Mm00493139_m1
TaqMan™ Gene Expression Assay (FAM), Mouse Il1r1	Thermofisher	Mm00434235_m1
TaqMan™ Gene Expression Assay (FAM), Mouse Il6	Thermofisher	Mm00446190_m1
TaqMan™ Gene Expression Assay (FAM), Mouse Alb	Thermofisher	Mm00802090_m1
TaqMan™ Gene Expression Assay (FAM), Mouse Il18	Thermofisher	Mm00434225_m1
TaqMan™ Gene Expression Assay (FAM), Human NLRP3	Thermofisher	Hs00918082_m1
TaqMan™ Gene Expression Assay (FAM), Mouse H2aa	Thermofisher	Mm00439211_m1
TaqMan™ Gene Expression Assay (FAM), Mouse H2ab1	Thermofisher	Mm00439216_m1
TaqMan™ Gene Expression Assay (FAM), Mouse Chil3	Thermofisher	Mm00657889_mH
TaqMan™ Gene Expression Assay (FAM), Mouse Nlrc5	Thermofisher	Mm01243039_m1
TaqMan™ Gene Expression Assay (FAM), Mouse Il1rn	Thermofisher	Mm00446186_m1
TaqMan™ Gene Expression Assay (FAM), Mouse Tnf	Thermofisher	Mm00443258_m1
TaqMan™ Gene Expression Assay (FAM), Mouse Nlrp12	Thermofisher	Mm01329688_m1
TaqMan™ Gene Expression Assay (FAM), Mouse Gfap	Thermofisher	Mm01253033_m1
TaqMan™ Gene Expression Assay (FAM), Mouse Il1b	Thermofisher	Mm00434228_m1
TaqMan™ Gene Expression Assay (FAM), Mouse Nlrp3	Thermofisher	Mm00840904_m1
TaqMan™ Gene Expression Assay (FAM), Mouse Casp1	Thermofisher	Mm00438023_m1
TaqMan™ Gene Expression Assay (FAM), Mouse Tmem119	Thermofisher	Mm00525305_m1
TaqMan™ Gene Expression Assay (FAM),Human 18s RNA	Thermofisher	H5999999-S1
hD305N mouse line	Snouwaert et al.[27]	N/A
hNLRP3 mouse line	Snouwaert et al.[27]	N/A
129S6/SvEv(mNlrp3)	Taconic	129SVE
MP-D305N mouse line	this paper	N/A

REAGENT or RESOURCE	SOURCE	IDENTIFIER
Oligonucleotides		
CGTCTGGATCAAGCTAAGAGAAC	Integrated DNA Technologies	MP-NLRP3 genotyping forward
TGCTTTCTCATAAAGGTCTCTCCTG	Integrated DNA Technologies	MP-NLRP3 genotyping reverse
Software and algorithms		
ImageJ (Rasband, NIH)	NIH	
QX Manager Software	Bio-Rad	https://ImageJ.nih.gov/ij/download.html
GraphPad Prism version 9.3.0	Graph Pad Software LLC	N/A
FlowJo Version 10.6.1	FlowJo, LLC, Ashland. CA	N/A